TECHNOLOGY DEVELOPMENT CENTER NEWS

COMMUNICATIONS RESEARCH LABORATORY

Serial No. 19 **November 2001**

CONTENTS

(continued on next page)

Second IVS General Meeting
February 4-7, 2002
Tsukuba, Japan

IVS 2002 General Meeting

hosted by
Geographical Survey Institute and
Communications Research Laboratory

The second IVS General Meeting will be held at Tsukuba International Congress Center (Epochal Tsukuba) in Tsukuba City, Ibaraki, Japan.

The third IVS Analysis Workshop will be held on February 8, following the General Meeting.

Registration deadline is January 10, 2002. (The abstract deadline was November 15, 2001.)

Visit the meeting web page at **http://ivscc.gsfc.nasa.gov/meetings/gm2002** or mirror web site (at CRL) **http://ivs.crl.go.jp/mirror/meetings/gm2002** for details.

Overview of the 1st CRL VLBI Technology Development Center Symposium

Tetsuro Kondo (*kondo@crl.go.jp*)

Kashima Space Research Center
Communications Research Laboratory
893-1 Hirai, Kashima, Ibaraki 314-0012, Japan

CRL has published the newsletter "IVS CRL-TDC News" twice a year in order to inform the development of VLBI related technology in Japan as an IVS technology development center to the world. The newsletter has been published based on reports presented at an internal meeting held at CRL twice a year. However only limited members attended this closed meeting from the outside CRL. Since April 1, 2001, CRL has become the independent administrative institution. We have taken this opportunity to change our meeting style from the closed meeting to an open symposium. CRL-TDC News will be published as proceedings of the symposium. According to this policy, the first CRL VLBI technology development center symposium was held at the Kashima Space Research Center on September 19, 2001. The symposium focused on recent VLBI related technology development and the status of current going on projects in Japan. Twenty-one papers were presented in the symposium.

The symposium started with a session of data processing, analysis, and observations. Followed by a session of technological development, real-time VLBI, and satellites and deep space. In the session of the observations, strong interferences at S-band due to a third-generation mobile phone system (IMT-2000) was reported. The third-generation system is the worldwide standard, so that geodetic VLBI receiving dual S and X bands will be seriously affected by this sytem in near future. Actually KSP-VLBI observations have been interfered at Koganei since July, 2001 due to a nearby transmitting station. In the session of satellites and deep space, two reports were presented concerning the positioning of Nozomi that is the first Japanese Mars spacecraft. In the report it was pointed out that delta VLBI technique was expected to play an important role on orbital determination of Nozomi for the final Earth swingby toward Mars planned in 2003. Moreover, a plan of the next generation space VLBI mission was also presented in the session. Importance of precise positioning of spacecraft was also pointed out in the report to achieve space VLBI at a millimeter wavelength. The symposium ended with a small banquet.

Attendance : Yuichi Ichikawa (Nitsuki), Takahiro Iwata (NASDA), Yoshihiro Fukuzaki (GSI), Md.M.R. Khan (Osaka Pref.U.), Hideki Ujihara (NAO), Hisashi Hirabayashi (ISAS), Tomoyuki Nakajo (Tohoku U.), Kentaro Ishizuka (UEC), Yoshiharu Asaki (ISAS), Shinobu Ymazaki (NTT-AT), Koji Hoshi (Matsushita EW), Eiichi Tanaka (SONY), Kiyoaki Wajima (ISAS), Makoto Yoshikawa (ISAS), Kenta Fujisawa (NAO), Sotesu Iwamura (NTT-AT), Tomonari Suzuyama (Kagoshima U.), Jun Amagai (CRL), Ryuichi Ichikawa (CRL), Eiji Kawai (CRL), Tetsuro Kondo (CRL), Mamoru Sekido (CRL), Hiroshi Okubo (CRL), Shinobu Arimura (CRL), Taizoh Yoshino (CRL), Yasuhiro Koyama (CRL), Hitoshi Kiuchi (CRL), Junichi Nakajima (CRL), Seiji Nagai (CRL), Fujinobu Takahashi (CRL), Hiroaki Umehara (CRL), Mizuhiko Hosokawa (CRL), Toshihiro Kubooka (CRL), Seiichiro Kawase (CRL)

The 1st CRL Technology Development Center symposium was held on September 19, 2001 at the Kashima Space Research Center. The symposium ended with a small banquet.

Comparative Time Series Analysis of the Radio Wave Intensity of the QSOs observed by VLBI (KSP) and GBI

Md. M. R. Khan[1]
(*mostafiz@mi.cias.osakafu-u.ac.jp*)
and N. Tanizuka[1,2]
(*tanizuka@mi.cias.osakafu-u.ac.jp*)

[1] *Graduate School of Science*
Osaka Prefecture University
1-1 Gakuen-cho, Sakai, 599-8531 Japan
[2] *College of Integrated Arts and Sciences*
Osaka Prefecture University
1-1 Gakuen-cho, Sakai, 599-8531 Japan

Summary: We present an experimental and comparative study on the dynamical structure of the galactic system. S band (2 GHz) and X band (8 GHz) flux densities of variable radio waves of various QSOs and BL Lacs from the GBI and the KSP VLBI are analyzed on the stand point of Higuchi's fractal dimension, Hurst exponent and the three dimensional phase space maps of the reconstructed time series.

1. Introduction

Variations of the intensities of extragalactic radio source have been studied for various sources [1,2]. The time series of the variable intensity of the radio wave from the QSOs at cosmological distance can be shown important information of the dynamics at the QSO system and of the evolution of the system. In this paper, the relationship between the fractal dimension, the Hurst exponent and the red shift, and the attarctors appearance on the phase space map are presented to discuss the informational structure on the evolution and the self-organization of the system.

The variation of the intensity may be influenced by various factors and changed from the original figure while it is transmitting through the space. The radio wave intensities of the quasars, BL Lacertaes and Galaxy are often variable with time span of days, weeks, months, years and so on. We want to approach the original figures of the intrinsic variations by some time series data analysis methods.

2. Data Analysis Method

2.1 Source Data

We have used about 1000 days' data from the followings -

1. July 1997 from VLBI observation under Key Stone Project (KSP) of Communication Research Laboratory[3,4]. The list of sources are shown in table 1.

2. February 1984 from GBI observation under NASA High Energy Astrophysics Program [5]. The list of sources are shown in table 2.

3. November 1996 from GBI observation under NASA High Energy Astrophysics Program [6,7]. The list of sources are shown in table 3.

Table 1. List of the quasars of VLBI observation from July 1997. Row 1, 2 and 3 are used to shown Source, Name and Red shift respectively.

0059+581	0316+413	0420-014	0552+398
	3C84		DA 193
	0.017	0.92	2.37
0727-115	0923+392	1226+023	1253-055
	4C39.25	3C273B	3C279
	0.70	0.16	0.54
1308+326	1334-127	1641+399	1730-130
		3C345	NRAO 530
1	0.54	0.59	0.90
1921-293	2134+004	2145+067	2251+158
OV 236			3C454.3
0.35	1.93	0.99	0.86

Table 2. List of the quasars of GBI observation from February 1984. Row 1 and 2 are used to shown Source and Red shift respectively.

0133+476	0202+319	0224+671	0235+164
0.860	1.466	0.524	0.851
0237-234	0333+321	0336-019	0420-014
2.224	1.253	0.852	0.915
0552+398	0828+493	0851+202	0923+392
2.365	0.548	0.306	0.699
0954+658	1245-197	1328+254	1328+307
0.368	1.275	1.055	0.849
1502+106	1555+001	1611+343	1641+399
1.833	1.770	1.404	0.595
1741-038	1749+096	1749+701	1821+107
1.054	0.322	0.760	1.036
2134+004	2200+420	2234+282	2251+158
1.936	0.070	0.795	0.859

2.2 Noise Elimination

We have used two methods for eliminating the noise based on the type of time series. They are:

1. Eliminate largest 10% of $X_n = \mid x_n$ - $\overline{x} \mid$, where $\overline{x}$ is the mean of all points x_n.

2. If ($x_j > x_{j-1} + \sigma$ and $x_j > x_{j+1} + \sigma$) or ($x_j < x_{j-1}$ - σ and $x_j < x_{j+1}$ - σ) then x_j is replaced by the average of x_{j-1} and x_{j+1}, where σ is the

Table 3. List of the quasars of GBI observation from November 1996. Row 1 and 2 are used to shown Source and Red shift respectively.

0224+671	0336-019	0851+202	0929+392
0.524	0.852	0.306	0.699
0954+658	1245-197	1328+254	1328+307
0.368	1.275	1.055	0.846
1741-038	200+420		
1.054	0.070		

standard deviation of the time series x_1, x_2, ..., x_j, ..., x_n, and n is the total length.

Figure 1 shows the original intensities of 0224+671 at 2.25 GHz and 8.3 GHz, and figure 2 shows the intensities after noise elimination.

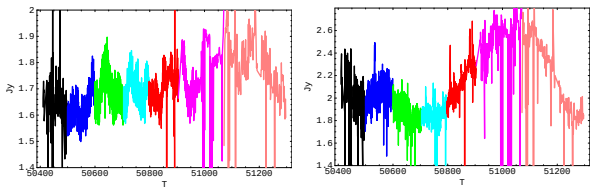

Figure 1. Original intensity of 0224+671 at 2.25 GHz (left) and 8.3 GHz (right)

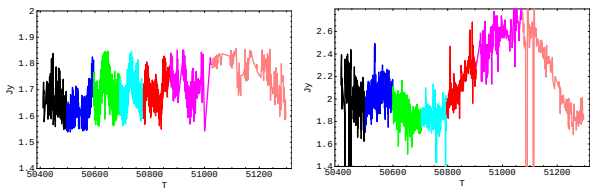

Figure 2. The intensity after noise elimination of 0224+671 at 2.25 GHz (left) and 8.3 GHz (right)

2.3 Phase Space Map

We plot the data of the time series in three-dimensional (3D) plane with various time lag, i.e., Lag 10, 20, 30 and so on. For plotting 3D graph we have taken X_t, X_{t+T} and X_{t+2T} through the axis x, y and z respectively. Here, T is the time lag and

$X_t = \{x_1, x_2, ..., x_i, ... x_{n-2T}\}$
$X_{t+T} = \{x_{1+T}, x_{2+T}, ..., x_{i+T}, ..., x_{n-T}\}$
$X_{t+2T} = \{x_{1+2T}, x_{2+2T}, ..., x_{i+2T}, ..., x_n\}$

Figure 3 shows the method of taking time lag graphically and we have taken the points like, $\{x_1, x_{1+T}, x_{1+2T}\}$, $\{x_2, x_{2+T}, x_{2+2T}\}$, ..., $\{x_i, x_{i+T}, x_{i+2T}\}$ and so on.
The attractors of the QSO 1226+023 (2C273B) at X band are shown in Figure 4. Figure 10 to 12 show the attractors appeared in some of the sources observed by VLBI (KSP).

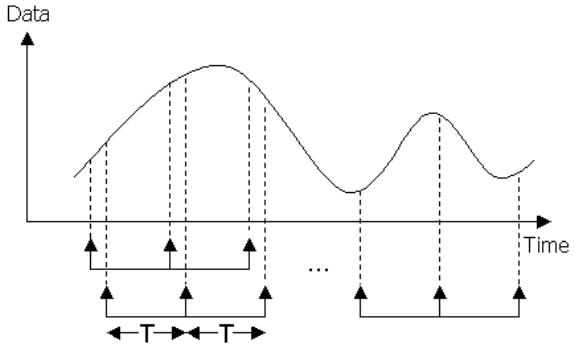

Figure 3. Method of taking time lag (T).

2.4 Hurst Exponent *H*

To calculate the Hurst exponent, we have used the Rescaled Range Analysis method of Hurst's Empirical Law.
The average influx over the period of τ days is
$\langle\xi\rangle_\tau = \frac{1}{\tau}\sum_{t=1}^{\tau}\xi(t)$
Let, X(T) be the accumulated departure of the influx ξ(t) from the mean $\langle\xi\rangle_\tau$.
$X(t,\tau) = \sum_{u=1}^{t}\{\xi(u) - \langle\xi\rangle_\tau\}$
The difference between the maximum and the minimum accumulated influx is the range R.
$R(\tau) = \max_{1\le t\le\tau} X(t,\tau) - \min_{1\le t\le\tau} X(t,\tau)$

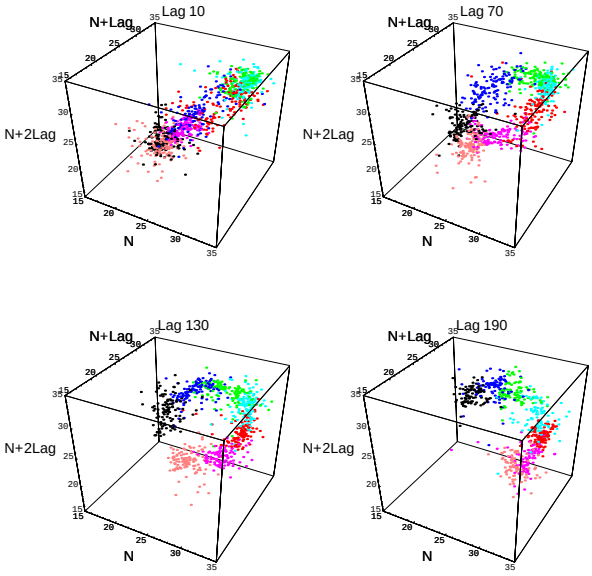

Figure 4. Three dimensional phase space map of 1226+023 (2C273B) at X band with various time lag.

Hurst used the dimensionless ratio R/S, where S is the standard deviation.
$S = \sqrt{(\frac{1}{\tau} \sum_{t=1}^{t} \{\xi(t) - \langle\xi\rangle_\tau\}^2)}$
Hurst found that the observed rescaled range, R/S, for many records in time is very well described by the following empirical relation -
$R/S = (\tau/2)^H$, where H is the Hurst exponent.
Figure 5 shows the method of calculating H graphically.

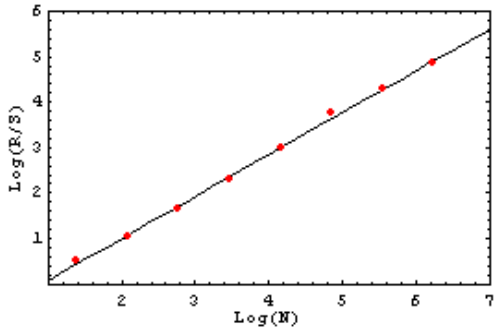

Figure 5. Graphical representation of calculating Hurst exponent of 0224+6712 at 2.25 GHz

2.5 Fractal Dimension D

To calculate the fractal dimension, D of the time series x(j): j = 1, 2, 3, ..., n, we have used Higuchi's method. We define a new time series as -
$x^m_{k,i} \equiv x(m + ik)$, i = 1, 2, 3, ..., M
The accumulated value of the absolute change in k (the sampling period) is normalized to sampling period 1 with
$M \equiv [\frac{n-m}{k}]$ ([ ] is the Gausian symbol, for example, [100.7] = 100).
$L_m(k) = \frac{1}{k} \frac{n-1}{Mk} \sum_{i=1}^{M} | x^m_{k,i} - x^m_{k,i-1} |$
Define L(k) to be the average value of L_m(k) for m = 1, 2, 3, ..., k, then
$L(k) \propto k^{-D}$, where D is called Higuchi's fractal dimension.
Figure 6 shows the method of calculating D graphically.

3. Relationships of Parameters

We have got interesting relationships between z, D and H. Figure 7 shows the relationship between z and D, figure 8 shows the relationship between z and H and Figure 9 shows the relationship between D and H.

4. Result and Discussion

In our analysis we have used different types of source data, i.e., KSP VLBI and GBI data. So, the base line of the source data is different. We have used GBI old and new data, i.e., the times of measuring intensity are different. We have also used X-band and S-band data, i.e., the band is also

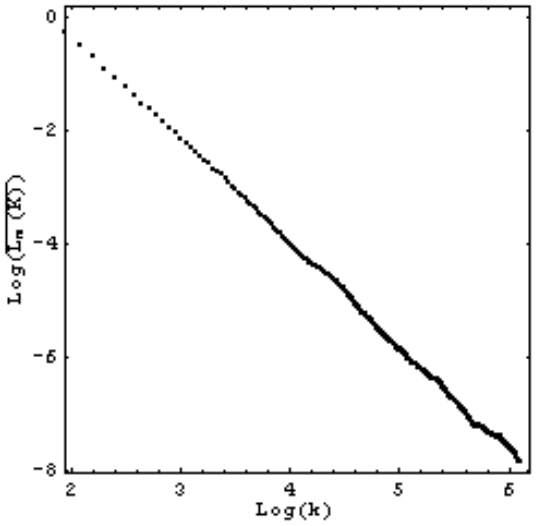

Figure 6. Graphical representation of calculating fractal dimension of 0224+6712 at 2.25 GHz

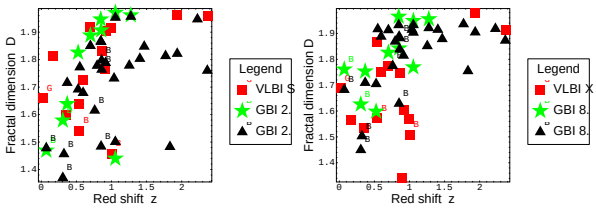

Figure 7. Relation between z and D at 2 GHz (left) and 8 GHz (right)

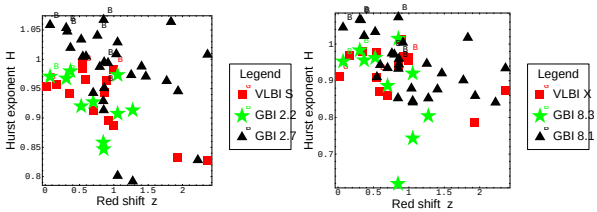

Figure 8. Relation between z and H at 2 GHz (left) and 8 GHz (right)

different. But in figure 7, we have found that the relationship between z and D is about same for all types of data. We have also found the same similarities in the relationship between z and H, and the relationship between D and H as shown in figure 8 and 9.

References

[1] R.L.Fiedler et al., Astrophys. J. Suppl. Ser. **65**, 1987, 319.

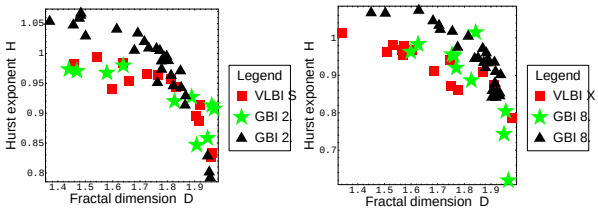

Figure 9. Relation between D and H at 2 GHz (left) and 8 GHz (right)

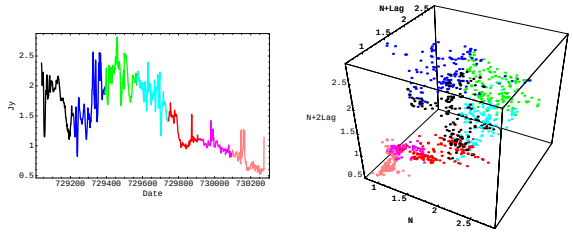

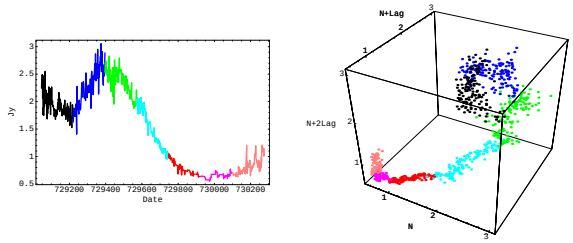

Figure 10. Source 0059+581, Lag 110 of S Band (up) and Lag 100 of X Band (down)

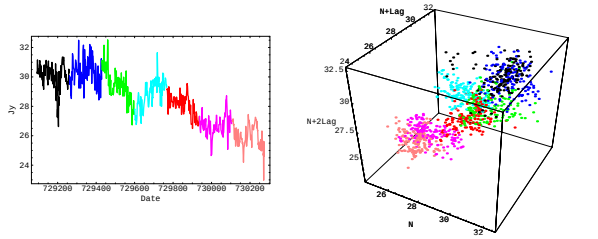

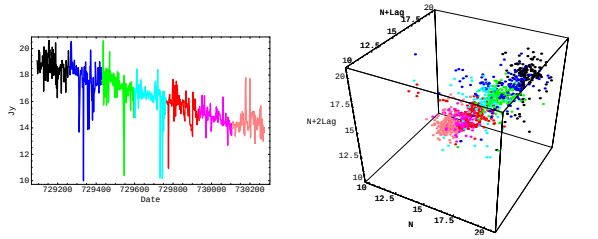

Figure 11. Source 0316+413 (3C84), Lag 70 of S Band (up) and Lag 70 of X Band (down)

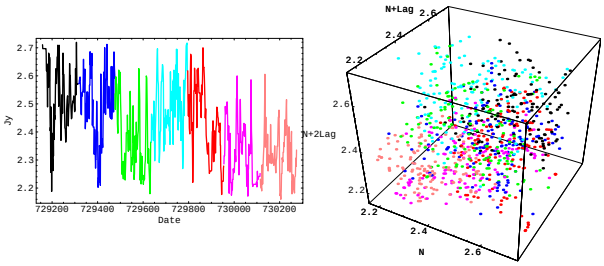

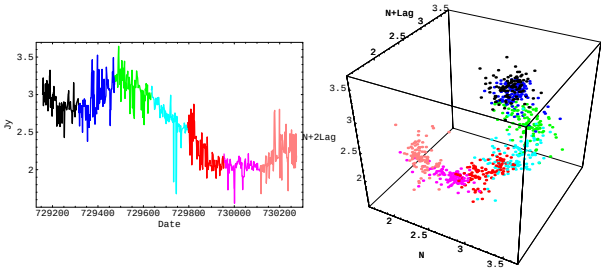

Figure 12. Source 0420-014, Lag 100 of S Band (up) and Lag 160 of X Band (down)

[2] E.B.Waltman et al., Astrophys. J. Suppl. Ser.**77**, 1991, 379.

[3] Y.Koyama, T.Kondo: Microwave flux density variations of compact radio sources monitored by real-time Very Long Baseline Interferometry, Radio Science, Vol. 36, No.2, pp.223-235, Mar./Apr. 2001. (also in Web site [4])

[4] http://ksp.crl.go.jp/index-j.html

[5] Trans. IEE of Japan, Vol.120-C,No.8/9,pp.1149-1156,Aug./Sep. 2000; N.Tanizuka, M.Takano: "Observational Study on a Process of Evolution of Galaxies," Proc. 15th Int. Conf. Noise in Physical Systems and 1/f Fluctuations, ed. C.Surya, Hong Kong, EDS-IEEE(Bentham Press,London,1999)pp.475-478,Aug.1999.pp.51-55;N.Tanizuka and M.Takano, "1/f Flctuations of the Intensity of Radio Wave from Compact Extragalactic Radio Sources,"Proc. 15th Int. Conf. Noise in Physical Systems and 1/f Fluctuations,ed.V.Bareikis et al.,pp.332-335,World Scientific,Singapore,1995.

[6] http://www.gb.nrao.edu/fgdocs/gbi/gbint.html*

[7] Md.M.R.Khan,N.Tanizuka:Time series analysis of the microwave intensity for the QSOs, in AB502, AP-RASC'01 URSI(Aug 1-4 2001,Tokyo, p 395);Causing Factors for the fluctuations of the radio wave from the QSOs.

*The Green Bank Interferometer is a facility of the National Science Foundation operated by the NRAO in support of NASA High Energy Astrophysics programs.

Status report of Working Group for Improving the KSP Correlation System

Yoshihiro Fukuzaki[1] (*fukuzaki@gsi.go.jp*), **Tetsuro Kondo**[2], **Mamoru Sekido**[2], **Hitoshi Kiuchi**[3], **Kazuhiro Takashima**[1], **and Kohei Miyagawa**[1]

[1] *Geographical Survey Institute*
Kitasato-1, Tsukuba, Ibaraki 305-0811, Japan
[2] *Kashima Space Research Center*
Communications Research Laboratory
893-1 Hirai, Kashima, Ibaraki 314-0012, Japan
[3] *Communications Research Laboratory*
4-2-1 Nukui-kita, Koganei, Tokyo 184-8795, Japan

1. Introduction

Correlation system developed by the Communications Research Laboratory (CRL) for Key Stone Project, which is called KSP Correlation system, was installed at the Geographical Survey Institute (GSI) in 1997, and has been used in order to process the data of domestic VLBI experiments (JADE sessions etc.). But there were some problems, which cause obstructions of regular processing in GSI. Therefore, Working Group was established at the 18th CRL TDC Meeting in order to improve the correlation system and started several activities.

2. Investigation and Improvement

The WG has researched and improved the following items.

1) A priori calculation

When the domestic experiments were processed with KSP Correlation system, it was recognized that fringes were not detected in some cases. After the investigation, it was found that a priori calculation was unsuitable in the case of no fringe detection. The following is an example.

Correct		
τ_g	:	1.5583505626E-04
τ_g/dt	:	-8.5759145115E-10
$d^2\tau_g/dt^2$	:	-8.9466416215E-13
$d^3\tau_g/dt^3$	:	4.5594133294E-18
Incorrect		
τ_g	:	1.5580446137E-04
$d\tau_g/dt$	:	-7.4562175872E-07
$d^2\tau_g/dt^2$	:	-5.2377946338E-08
$d^3\tau_g/dt^3$	:	-3.5076813218E-10

The values of $d\tau_g/dt$ are different more than 3 orders. This was a cause of no fringe detection. The reason of this miscalculation is that a priori calculation was designed for the same durations in an observation, and in the case that the durations are different, miscalculation occurs. In order to avoid this problem, we changed the scheme of a priori calculation. But there is still uncertainly of a priori value, so coherent loss may occurs. We have to solve this problem.

2) GPIB-RS422 protocol converter for Automatic Tape Changer

GPIB-RS422 protocol converter for Automatic Tape Changer sometimes hung up during the correlation. Program bug was the cause of this. We revised the program in the ROM that controls SRQ process.

3) Failure of synchronization of recorders

Failure of synchronization of recorders sometimes occurred. In order to avoid this problem, we changed the parameter of time stamp mode from t=0 to t=15. The change effects that the data of the top of recording for 15 seconds is suppressed (data=00), and only time stamps are recorded. Failure of synchronization of recorders was decreased sharply by this modification.

4) Misclosure of phase delay

Dr. Leonid Petrov of NASA/GFSC found out the misclosure of phase delay produced by KSP correlation system. The example is shown in Figure 1 and Figure 2. We are now investigating this issue.

5) Q code

Q code in the output of Mark IV system is now 2 digits, but KSP's is 1 digit. The output format has been modified by Haystack and GSFC year by year, but in Japan it has not been done. This issue causes some problems when we analyze with SOLVE. We are now investigating this issue.

3. Summary

The WG started an activity to improve KSP correlation system. Some issues were investigated and some problems were solved. WG aims to make KSP correlation system perfect.

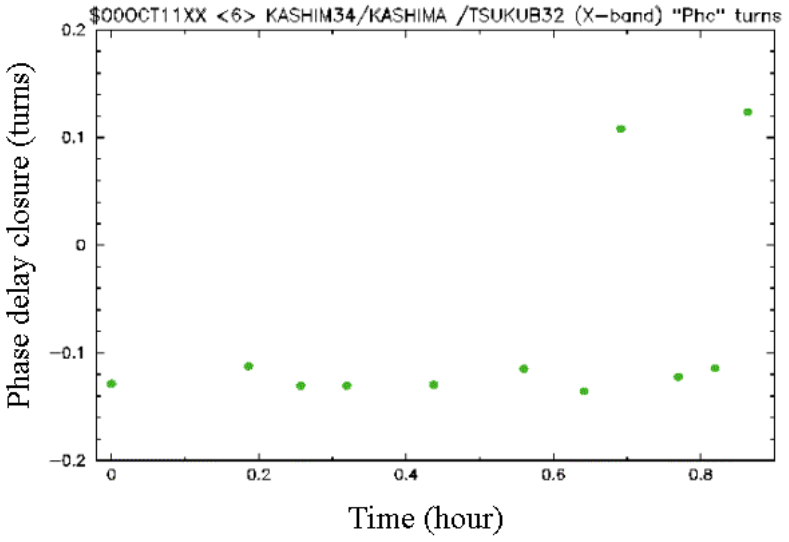

Figure 1. Phase delay closure of the data produced by KSP system.

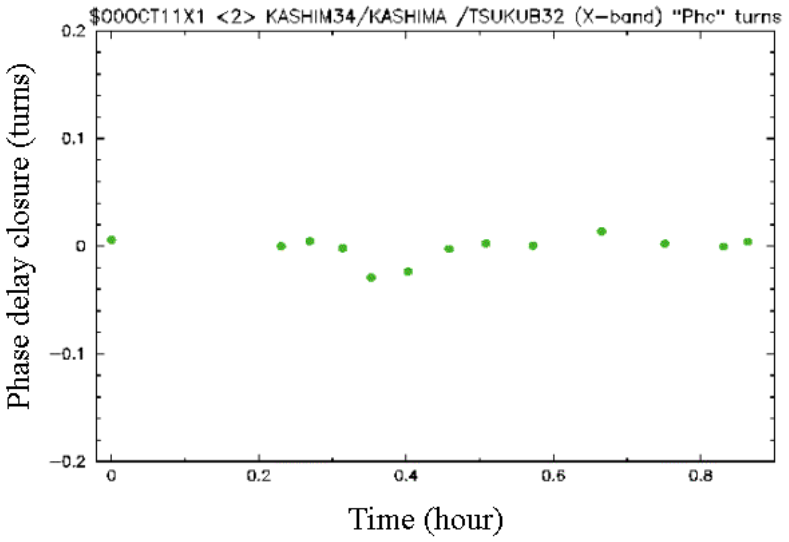

Figure 2. Phase delay closure of the data produced by Mark IV system.

The signal of a third-generation mobile system, IMT-2000, jams KSP VLBI observation

Jun AMAGAI(*amagai@crl.go.jp*), **Hitoshi KIUCHI, and Koichi SEBATA**

Communications Research Laboratory
4-2-1 Nukui-kita, Koganei, Tokyo 184-8795, Japan

Since 1996, the Communications Research Laboratory has been conducting the Keystone Project (KSP) to monitor crustal deformation around the Tokyo metropolitan area using three space geodetic techniques, VLBI, SLR, and GPS. Recently, VLBI observation at the KSP Koganei station experienced quite heavy radio interference in the S-band. Figures 1 (a) and (b) show the spectra of the RF and IF signals received at the Koganei station. We can see heavy interference at 2.14 GHz. The RF low noise amplifier was not saturated, however the IF amplifier was saturated and the noise floor level of the amplifier was suppressed. We were forced to change the frequency arrangement to eliminate this interference. Though a filter is needed to avoid IF saturation, we have not got a suitable one yet.

We investigated the source of the interference and found that it was a signal that came from a telecommunications radio tower, 900 m from the Koganei station. On July 2, 2001, the company started transmitting IMT-2000 test signals and since then the interfering signal has jammed our observation. The specifications of the transmission station are listed in Table 1. The incident power flux of the signal at our antenna is estimated to be very high. The company is planning to extend the IMT-2000 network to every major city in Japan before April 2002. Since other countries face a similar situation, VLBI stations in many countries will likely be jammed by IMT-2000 signals and be forced to take measures to deal with the interference.

IMT-2000: The global-standard for third generation wireless communications (http://www.imt-2000.org/portal/index.asp).

Table 1. Specifications of IMT-2000 station near KSP Koganei station

Frequency:	2137.6 - 2147.4 MHz (50 bands with 200 kHz spacing)
Modulation:	G7W
Antenna power:	16 W
Antenna gain:	21 dB
Antenna height:	57.8 m

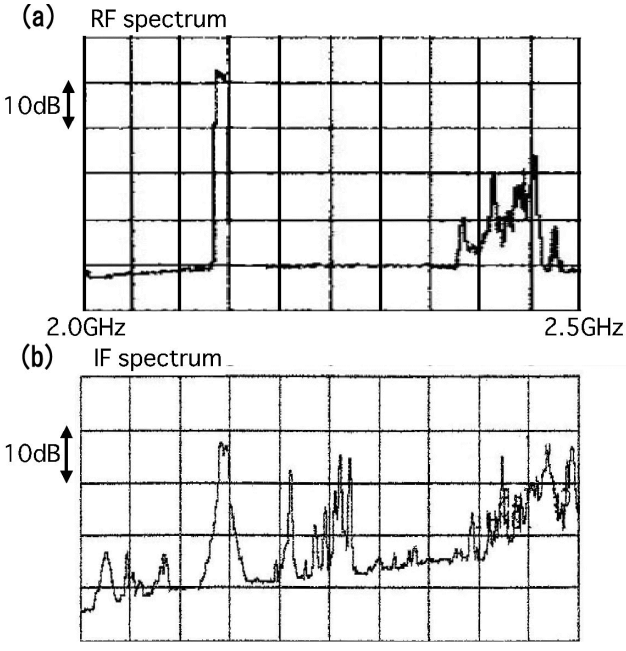

Figure 1. (a) Spectra of RF signals obtained when the antenna was directed towards the zenith at a maximum hold integration of 30 minutes. (b) Spectra of IF signals obtained using maximum hold integration during 24 hours of VLBI observation.

A Plan of Improving Reception Efficiency of 43 GHz Observation at Kashima 34-m Antenna

Eiji KAWAI (*kawa@crl.go.jp*), **Hiroshi OKUBO, Hiro OSAKI, Junichi NAKAJIMA, and Tetsuro KONDO**

Kashima Space Research Center
Communications Research Laboratory
893-1 Hirai, Kashima, Ibaraki 314-0012, Japan

1. Introduction

Although the pointing error and decrease in receiving efficiency of the 34-m antenna at Kashima are small for reception at 22 GHz, they are suppose to be large at 43 GHz. We investigated two factors that cause efficiency decreases at 43 GHz. One is an antenna pointing calibration error. The other is an effect of subreflector displacement due to gravitational deformation of quadripod and also due to its thermal expansion. Consequently we found that the subreflector position should be controled to compensate the displacement due to gravitational distortion of quadripod. Comparing with this gravitational effect, an antenna pointing error is a miner cause. However it should be improved to attain the higher efficiency.

2. Antenna pointing calibration error

The half-power beam width (HPBW) of the 34-m antenna at 43 GHz is 0.014°, which means that 0.007° pointing error causes the signal strength decrease of 3 dB under the assumption of the Gaussian beam pattern. We estimated the decrease in efficiency from current pointing calibration errors and HPBW at 43 GHz. Current azimuthal and elevational pointing root-mean-square errors after pointing calibration are 0.0033° and 0.0022°, and causes 14 % and 7 % efficiency dcreases, respectively. Sinusoidal component of the difference in the azimuth-rail level is already modeled in the pointing calibration, however a stepwise displacement sometimes seen at the Kashima 34-m antenna is not well-modeled. We estimated the level difference effect on the efficiency decrease as follows.

The radius of the azimuth rail is 9.8 m. We assume the level difference on the rail of 1 mm. Thus, if the elevation angle is directly affected, pointing error reaches a maximum of 0.0045°, and the efficiency decrease reaches a maximum of 25%. However the wheel direction is separated by 39.2° from a horizontal beam direction. Hence the height change of a wheel does not directly affect the beam elevation angle. We corrected this effect using a simple relation ($\cos(39.2°) = 0.77$) and obtained 0.0045° elevation pointing error. Results are summarized in Table 1.

Table 1. Pointing calibration error and estimated efficiency decrease at 43 GHz.

Pointing error	Efficiency decrease (%)
AZ 0.0033° (rms)	14
EL 0.0022° (rms)	7
Level difference on azimuth rail 1 mm → 0.0045° (max)	25

In the meantime, the antenna is supported by four wheels, so the direction change of antenna beam is thought to be a complicated relation with the height change of each wheel. To obtain actual structual deformation, we are planning to measure the inclination by using an inclinometer. Preliminary measurement results are described in another report in this issue [*Okubo et al.*, 2001]. Furthermore to improve the pointing calibration, we will add new parameters to a pointing calibration model.

3. Effect of focus displacement

3.1 Gravity deformation of subreflector quadripod

The subreflector of the antenna is supported by a quadripod. Gravity deformation of the quadripod causes the efficiency decrease of the antenna. Observations at 22 GHz shows that efficiency changes

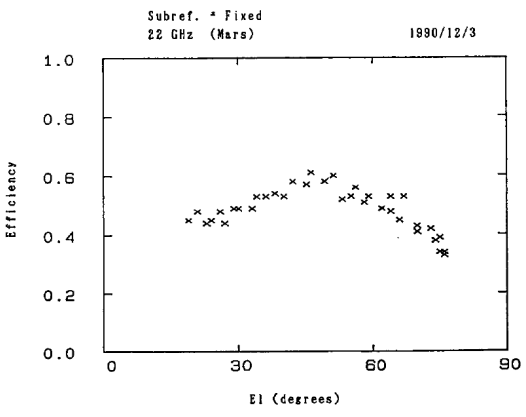

Figure 1. Efficiency of 34-m antenna at 22 GHz when subreflector is fixed at the best position (45° elevation) [Takaba, 1991].

as a function of elevation angle if the position of a subreflector is fixed at the best position obtained at 45° elevation (Figure 1). We converted the decrease in efficiency to that for 43 GHz simply using the frequency ratio. Table 2 shows the decrease in efficiency at 43 GHz for three different elevation angles.

Table 2. Decrease in antenna efficiency at 43 GHz when elevation angle is changed. Subreflector position is fixed at best position obtained at 45° elevation.

Elevation angle	Efficiency decrease (%)
45°	0
60°	35
70°	66

When the subreflector is fixed to the best position obtained at 45° elevation, the efficiency decreases greatly as the elevation angle separates from 45°. The displacement of subreflector by 5 mm in Y-axis (perpendicular to the beam direction) corresponds to a beam elevation-angle offset of 1 arc minute at the Kashima 34-m antenna. Thus a beam offset of 0.001° is attributed to about 0.3 mm displacement of the subreflector in Y-axis. This can occur easily by the gravitational effect. According to our numerical simulation, the displacement of subreflector in Y-axis causes not only a beam offset but also an efficiency decrease due to a defocus effect.

3.2 Thermal deformation of subreflector quadripod

The position of the subreflector changes as the quadripod support expands and/or contracts as the temperature changes. The temperature expansion coefficient of iron is 11.8×10^{-6}/°C. The length of quadripod is about 5.4 m. Therefore a temperature change of 20°C yields 1.3 mm shift of subreflector along the beam axis. We measured the efficiency decrease at 22 GHz due to the subreflector shift and got a efficiency changing rate of 5%/mm, which corresponds to 10%/mm at 43 GHz. Therefore, the decrease in efficiency at 43 GHz will become 13% for a 1.3 mm position shift.

4. Summary

We have estimated the effect of the pointing calibration errors and subreflector displacement on the reception efficiency at 43 GHz. The amount of efficiency decrease due to the pointing calibration errors was calculated under the assumption of Gaussian beam pattern. The subreflector displacement effect was estimated from the gravitational effect and thermal expansion effect independently. An estimation of the efficiency decrease at 43 GHz was simply made from the observational data taken at 22 GHz by merely considering the frequency difference ratio. The efficiency decreases estimated this way are summarized in descending order in Table 3.

Table 3. Estimated decrease in efficiency at 43 GHz in descending order.

Causes	Efficiency decrease (%)
Gravity deformation of subreflector quadripod	
at 70° EL	66
at 60° EL	35
Level difference of AZ rail (1 mm)	25
Pointing calibration error	14
Subreflector displacement due to thermal expansion (ΔTemperature= 20°C)	13

As shown in Table 3, the displacement of subreflector due to the gravitational effect causes larger efficiency decrease than other causes such as the pointing calibration error. This means that the compensation of the subreflector displacement is an important factor to increase the efficiency at 43 GHz observations.

We conclude that a subreflector control system is necessary to keep high receiving efficiency at all elevation angles. The 34-m antenna has a subreflector control system and it used to be worked. However it has been malfunctioned due to aging of the system. Therefore a new PC-based system to control the 5-axis subreflector control mechanism is being developed now. The system eanables us to adjust the displacement of the subreflector as a function of the elevation angle.

References

Okubo, H., E. Kawai, T. Kondo, H. Osaki, J. Nakajima, and K. Ishizuka,"Inclinometer Measurement of Kashima 34m antenna – Preliminary Report –", IVS CRL-TDC News No.19 (this issue), pp.13-14, 2001.

Takaba, H., "VLBI Antennas of the Communications Research Laboratory", J. Commun. Res. Lab., Vol.38 No.3, pp. 417-433, 1991

Inclinometer Measurement of Kashima 34m antenna – Preliminary Report –

Hiroshi Okubo (*okubo@crl.go.jp*), **Eiji Kawai, Tetsuro Kondo, Hiro Osaki, Junichi Nakajima, and Kentaro Ishizuka***

Kashima Space Research Center
Communications Research Laboratory
893-1 Hirai, Kashima, Ibaraki 314-0012, Japan
* *The University of Electro-Communications*

1. Introduction

Kashima 34-m radio telescope has been installed 43-GHz receiver. 43-GHz Observation requires higher accuracy of antenna control toward the certain point on the sky. Kashima 34-m radio telescope operating system has 11 parameters of pointing model, but even if we obtained pointing parameter of minimum error, pointing accuracy of antenna is still uncertain. Because Kashima 34-m radio telescope has concern of unevenness of azimuth rail. Solving this problem, we measured actual antenna movement using inclinometer. In this paper we will introduce inclinometer measurement system and preliminary result.

2. Measurement system

The inclinometer made by Applied Geomechanics Inc. of U.S.A., model 711-2A has X and Y-axis level sensor and equipped temperature sensor. Detected actual tilts converted to ±8 V DC output signal. If inclinometer set on complete leveled plane, the inclinometer output is 0 V. The inclinometer has High and Low gain output mode. This function made possible to switch tilt sensor range corresponding with various measurement purpose. (Table 1) Inclinometer equipped with low pass filter to reduce higher frequency noise.

Table 1. Inclinometer specifications.

Range	High : ±400μRadian Low : ±4000μRadian
Output	High : 50μRadian/Volt Low : 500μRadian/Volt

To embed inclinometer on the antenna structure rigidly, we made base mount with level adjusting screw (Fig. 1) .

DC output signals are fed to DAT recorder, and recorded 5 kHz sampled 16-bit digital signal.

Figure 1. Inclinometer embedded on antenna structure.

Recorded data is processed by workstation. Two inclinometer are embedded on the antenna structure of both side of elevation axis. Y-axis of inclinometer is corresponding with elevation tilts direction and X-axis is match with level of elevation axis (Fig. 2).

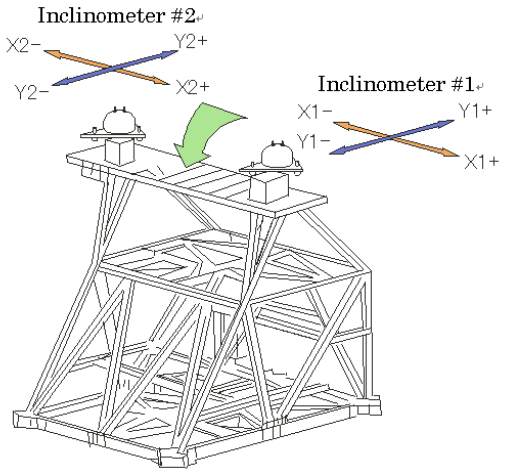

Figure 2. Embedded inclinometer on 34-m antenna elevation axis.

We have carried out measurement of Kashima 34-m radio telescope with this system on September 17 of 2001. Inclinometer was set High gain mode and low pass filter was turned on. To measure unevenness of azimuth rail, the antenna rotates azimuth 360° per 2 hours (0.05°/sec). We repeated the same measurement two times opposite direction to confirm repeatability of collected data.

3. Result and Discussion

Collected data is transferred to workstation and averaged. Figure 3 shows the processed result of in-

clinometer#1 1st and 2nd time measurement. We can see good repeatability on both axes. Data contains continues bumps, we assumed it is cause of unevenness of azimuth rail joints.

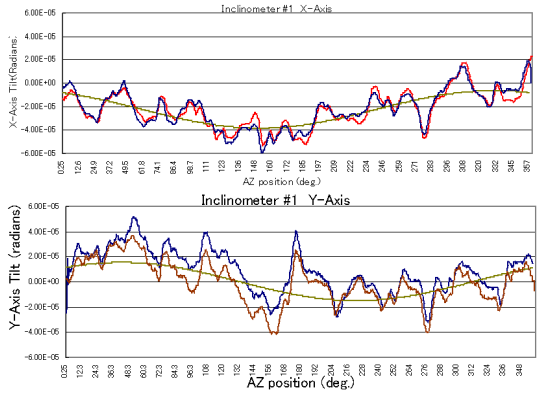

Figure 3. Repeatability of inclinometer data.

Fitted sin curve has approximately 90° phase difference between both axes. This fact suggests azimuth plane is slightly tilted toward certain direction and inclinometer detects azimuth plane tilt in X and Y axes. To evaluate acquired inclinometer output data, we compared with the pointing model parameter of antenna operating system. The parameter of azimuth plane tilts is calculated and plotted (Figs. 4,5).

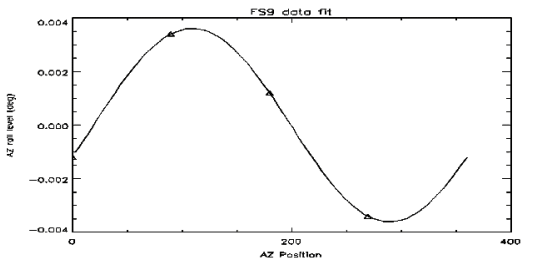

Figure 4. Current antenna operating system (FS9) pointing model parameter.

Compared with inclinometer Y-axis output, FS9 and NKAOS, All three plots show agreement, but inclinometer data has approximately 50° phase difference. We assumed inclinometer data are reliable and showing as good sensitivity as pointing parameter.

4. Conclusions

To improve pointing accuracy of Kashima 34-m radio telescope, we measured antenna movement using inclinometer embedded on elevation axis.

We concluded as following.

- Inclinometer detects azimuth rail unevenness and azimuth plane tilts with good repeatability and sensitivity.
- Comparing detected azimuth plane tilts and current pointing model parameter agreed.

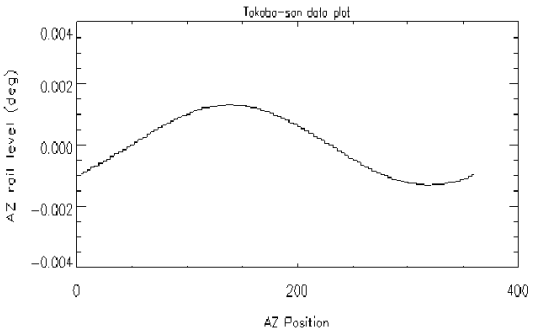

Figure 5. Former antenna operating system (NKAOS) pointing model parameter.

Applying inclinometer data, we are planning to review current pointing model and create new pointing model that consider azimuth rail unevenness or other local conditions.

Reference

Gawronski W., Baher F., Quintero O., “Azimuth-Track Level Compensation to Reduce Blind-Pointing Errors of the Deep Space Network Antennas” IEEE Antennas Propag. Mag., Vol42 , No2, April 2000

MarkIV Field system Documentation, “Pointing Model” Ver.8.2., Sept. 1, 1993

Takaba, H., “VLBI Antennas of the Communications Research Laboratory”, J. Commun. Res. Lab., Vol.38 No.3, pp. 417-433, 1991

Development of the radiometric phase correction method using a 22-GHz water vapor line radiometer

Yoshiharu Asaki[1] (*asaki@vsop.isas.ac.jp*), **H. Kobayashi**[2], **M. Ishiguro**[2], **H. Hirosawa**[1], **and H. Hirabayashi**[1]

[1] *Institute of Space and Astronautical Science 3–1–1 Yoshinodai, Sagamihara, Kanagawa 229–8510, Japan*
[2] *National Astronomical Observatory 2–21–1 Osawa, Mitaka, Tokyo 181–8588, Japan*

1. Introduction

Phase stability in radio interferometry is an important issue both for high quality imaging and the detectability of celestial radio sources. However, atmospheric phase fluctuations due to the water vapor content degrade the imaging performance and cause coherence loss, resulting in the sensitivity degradation. Phase compensation techniques to solve the problem are required for current and future millimeter- and submillimeter-wave interferometry, such as ALMA. One of the promising techniques is a differential radiometric phase correction method, which makes use of a correlation between the brightness temperature and the Excess Path Length (EPL) of the atmospheric water vapor (Welch 1999). The coherence of the interferometry phase can be successfully improved with the radiometric phase correction (Resch et al., 1984; Bremer et al., 1997).

The Institute of Space and Astronautical Science (ISAS) launched a radio astronomy satellite, named HALCA (the Highly Advanced Laboratory for Communications and Astronomy), in 1997 (Hirabayashi et al., 1998). A highly stable frequency standard for HALCA is supplied from a ground tracking station via a phase-transfer system while the observation data is transmitted back to the station. Since the atmospheric phase fluctuations along a single line of sight are seen in the round trip phase of the downlink signal, we can directly compare the phase fluctuations with the atmospheric brightness temperature. In this paper, we introduce the water vapor line radiometer to measure the 22-GHz line emission to be mounted on the 10-m diameter parabolic antenna of the tracking station at Usuda, Japan. The satellite tracking passes are scheduled at various times and elevations. In this study, we can investigate how to determine a scale factor to convert the vapor brightness temperature to the EPL, which is very dependent on meteorological conditions such as the atmospheric temperature, pressure, and humidity. This means that the scale factor may be variable with time, antenna site, and observing elevation angles. If the radiometric phase correction is to be used for radio interferometers, we have to know how sensitive to observing conditions the scale factor is. In section 2, we will show some basic concepts of this study, introducing the HALCA phase-transfer system and the radiometer. The current status of the data analysis is described in section 3.

2. Basic concepts

2.1 Phase-transfer system of HALCA

HALCA is a radio astronomy satellite with an 8-m diameter deployable antenna to observe celestial radio sources at 1.6 and 5 GHz. HALCA has been operated under the international VLBI Space Observatory Programme (VSOP) with the collaboration of many organizations and ground radio telescopes around the world.

In general, VLBI telescopes are equipped with a very highly stable frequency standard generated from an atomic maser. In the case of HALCA, the frequency standard is supplied by an uplink carrier signal at 15.3 GHz phase-locked to a hydrogen maser from the ground tracking station. The tracking network consists of five stations: three of the Deep Space Network (Goldstone in the USA, Madrid in Spain, and Tidbinbilla in Australia), one of the National Radio Astronomy Observatory (Green Bank in the USA), and one of ISAS (Usuda in Japan). The frequency of the uplink signal is controlled at the tracking station to compensate for the spacecraft Doppler shift due to its orbital motion so that it is received at 15.3 GHz onboard.

Onboard reference signals used for frequency and analogue-to-digital conversions of radio waves from celestial sources are all generated from the uplink signal. The Quadrature Phase Shift Keying modulated data is transmitted at 128 Mbps to the ground tracking station at 14.2 GHz (Kobayashi et al., 2000). The frequency of the received downlink signal is also Doppler-shifted. This frequency shift is compensated for at the tracking station, and the VLBI data is recorded on magnetic tapes.

2.2 A line radiometer onto the HALCA tracking antenna

Our line radiometer was designed to receive atmospheric microwave radiation from 19.15 to 26.35 GHz to monitor the water vapor content at Usuda (∼1400-m altitude site) where the humidity is

rather high. The received signal is divided into eight frequency channels, each with 900-MHz bandwidth (Asaki et al., 2000). A standard power with the equivalent noise temperature of about 300 K generated by a noise diode is injected at a point between the feed horn and the first LNA. The system noise temperature is calculated using so-called a Y-factor method, in the a ratio between the powers with the noise diode switched on and off is obtained to cancel the gain fluctuations of the LNAs of the radiometer. The atmospheric brightness temperature can be obtained by subtracting the receiver noise temperature which is already measured.

The line radiometer is mounted close to the Cassegrain focus of the 10-m dish of the tracking antenna. The radiometer's line of sight is about 0.6 degree from the beam of the satellite communication link. This angular offset corresponds to a spatial separation of 11 m at 1-km. Assuming the wind velocity aloft is 10 m/s, the transverse time is nearly one second. The angular offset is negligible when we compare the round trip phase with the brightness temperature averaged for greater than a few seconds.

2.3 Comparison between round trip phase and water vapor brightness

We use the following equation to obtain the one-way EPL fluctuation due to the water vapor, ΔL_w,

$$\Delta L_w = \frac{c\Delta\Phi_w}{\omega_d + \omega_u}, \tag{1}$$

where $\Delta\Phi_w$ is the round trip phase fluctuation due to the water vapor in radians, c is the speed of light, and ω_u and ω_d are angular frequencies of the uplink ($2\pi\times$15.3 GHz) and downlink ($2\pi\times$14.2 GHz), respectively. ΔL_w is proportional to the integration of the column density of the water vapor content along the path of the transmitted radio wave (Thompson et al., 2001). Note that $\Delta\Phi_w$ is a summation of contributions of the uplink and downlink signals.

From the radiative transfer equation, the sky brightness temperature T_B is given by,

$$T_B = T_{atm}(1 - e^{-\tau}), \tag{2}$$

where T_{atm} and τ are the atmospheric physical temperature and opacity, respectively. We can assume $\tau << 1$ at frequencies around 22 GHz, so that equation (2) can be approximated by:

$$T_B = \tau T_{atm}. \tag{3}$$

Here, τ can be separated into three parts: contributions from dry air τ_d, water vapor τ_w, and liquid water (cloud) τ_l,

$$\tau = \tau_d + \tau_w + \tau_l. \tag{4}$$

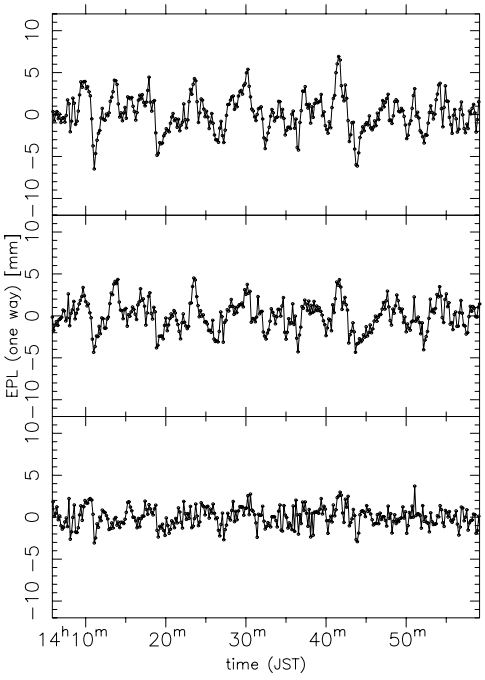

Figure 1. Time variations of the EPL calculated from the round trip phase (top), water vapor brightness (middle), and their difference (bottom). The experiment was conducted on 26 October, 2000.

Since each of the above components is proportional to the integration of the column density of each content along the line of sight, ΔL_w given in equation (1) is proportional to the fluctuation of $\tau_w T_{atm}$. One of the problems of radiometric phase correction is that rapid fluctuations in the measurement of the atmospheric brightness temperature are caused by the liquid content ($\tau_l T_{atm}$) when cloud covers over an antenna site although it does not affect to the atmospheric EPL. Assuming cloud is not present, we obtain the following relation,

$$\Delta\Phi_w = \frac{\omega_d + \omega_u}{c}\cdot\alpha\cdot\Delta T_{Bw}. \tag{5}$$

Here, α is the scale factor to convert the fluctuation of the measured brightness temperature due to the water vapor ΔT_{Bw} to ΔL_w. The factor is typically 6 mm/K for the water vapor emission peak at 22.235 GHz, although it depends on meteorological conditions and elevation angle very much.

3. Data analysis

We calculated the EPL using the round trip phase with equation (1). Since a fast phase rotation, greater than a few Hz, due to the residual Doppler remained in the original round trip phase,

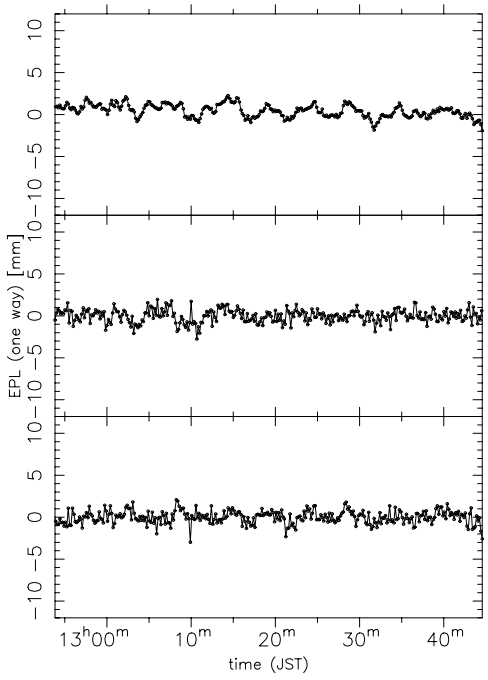

Figure 2. Time variations of the EPL calculated from the round trip phase (top), water vapor brightness (middle), and their difference (bottom). The experiment was conducted on 4 November, 2000.

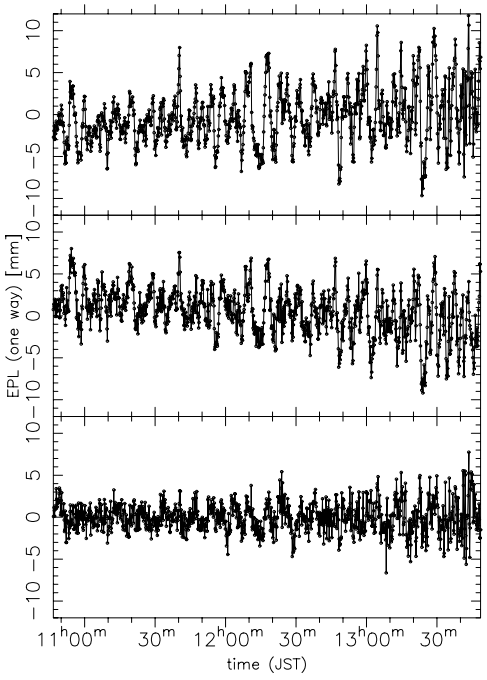

Figure 3. Time variations of the EPL calculated from the round trip phase (top), water vapor brightness (middle), and their difference (bottom) on 23 November, 2000.

rapid time variations were removed by subtracting a smooth curve estimated from a cubic spline interpolation of 400-sec averaged time series. The data was then averaged for 10 seconds after a bias and linear trend estimated by a least squares fitting were removed.

The atmospheric brightness temperature calculated from the Y-factor was first averaged for 10 seconds for each of the frequency channels. The central three channels covering 20.95–23.65 GHz were then averaged each 10 seconds. A smoothing curve estimated from a cubic spline interpolation of 400-sec averaged time series was also removed. Then a bias and linear trend estimated by a least square fitting were removed. To convert the atmospheric brightness to the EPL, the scale factor α was determined to minimize the Root Mean Square (RMS) value of the EPL difference between the two time series for each of the experiments. If the scale factor could not be determined for some reason, we used the value of 6 mm/K as a default to compare the two time series.

The first experiment was conducted on October 26, 2000, when it was a little cloudy. Figure 1 shows the time variations of the one-way EPL calculated from the round trip phase in the top plot, the atmospheric brightness temperature in the middle, and the difference between the two time series in the bottom. We adopted the scale factor of 6.6 mm/K for this experiment, which minimizes the RMS of the EPL difference. Figure 2 shows the time series on November 4, 2000, when it was very fine. Since the EPL fluctuation was originally very small as well as the atmospheric brightness, the correlation of the two time series was not very strong. We could not determine the suitable scale factor, and so the default value was used for the comparison. Figure 3 shows the results of the experiment on November 23, 2000, under a clear sky.

Table 1. Scale factors to convert the atmospheric brightness temperature to the EPL and RMS of the differences between the round trip phase and atmospheric brightness temperature.

Date (2000)	Scale Factor [mm/K]	EPL difference [mm]
Oct 26	6.6	1.2
Nov 4	6.0*	0.8
Nov 23	8.3	1.8
Nov 27	6.0*	8.4

* default scale factor.

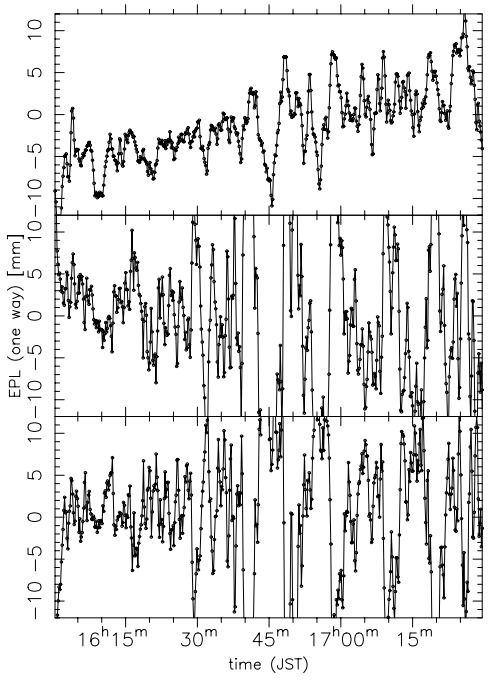

Figure 4. Time variations of the EPL calculated from the round trip phase (top), water vapor brightness (middle), and their difference (bottom) on 27 November, 2000.

We adopted the scale factor of 8.3 mm/K. The scale factors and RMS of the EPL differences for the experiments described here are listed in Table 1

On the other hand, when the weather conditions were not good, the correlation of the two time series was worse. Figure 4 shows the results of the experiment conducted on November 27, 2000, when it was cloudy and antenna site were enshrouded by thick fog, and snow started to fall after the experiment finished. Since a good correlation could not be found, we used the default scale factor for the comparison. We consider that much larger fluctuations in the atmospheric brightness can be attributed to the presence of the thick cloud covering the antenna site. This large brightness fluctuation will be almost removed by making use of the frequency channels away from the emission peak: the common time variation due to the liquid content will be canceled by differencing the channels between the emission peak and wings (Marvel and Woody, 1998). We are currently developing such an algorithm to achieve a more precise phase correction with our radiometer.

References

Asaki, Y., Kobayashi, H., Hagiwara, N., and Ishiguro, M. 2000, SPIE 4015, 589

Bremer, M., Guilloteau, S., and Lucas, R. 1997, in Science with large millimeter array, P. Shaver Ed., 3357, 240

Hirabayashi, H. et al. 1998, Science, 281,1825

Kobayashi, H., et al. 2000, PASJ, 52,967

Resch, G., Hogg, D., and Napier, P. 1984, Radio Sci., 19, 411

Thompson, A., Moran, J., and Swenson, G. 2001, In Interferometry and synthesis in radio astronomy (2nd Edition), A Wiley–Interscience publ.

Welch, J. 1999, Review of Radio Sciences, URSI, 787

Evaluation of the double frequency interferometer method applied for the long baseline observations of the Jovian decametric radiations

Tomoyuki Nakajo[1]
(*nakajo@stpp1.geophys.tohoku.ac.jp*), **Takayuki Ono**[1], **Masahide Iizima**[1], **Masaru Oya**[1], **and Hiroshi Oya**[2]

[1]*Department of Geophysics, Graduate School of Science, Tohoku University*
[2]*Fukui University of Technology*

1. Introduction

Jovian decametric radiations (DAMs) are the most intense non-thermal planetary radio emissions in the solar system which are generated in the magnetized plasmas in the planetary magnetosphere. DAMs are generally supposed to be generated at the frequency from 10 to 40 MHz, which is very close to the local electron cyclotron frequency of the source region with altitude up to about 0.5Rj in the Jovian polar ionosphere. Since the discovery of Jovian aurora by the extreme ultraviolet spectrometer on board Voyager 1 [*Broadfoot et al.,* 1979], it has been considered that these DAMs are generated in close relationship with these auroral phenomena as is the case of auroral kilometric radiations (AKRs) from the Earth.

Considering the high radiation power of DAMs with the maximum energy up to 10^11[W], contribution of coherent plasma wave processes including "wave-particle interactions" is essential to explain the generation mechanism. Two wave-particle interaction mechanisms have been proposed to explain the strong DAM emissions; one is "direct mechanism" and the other is "indirect mechanism". As the direct mechanism the Cyclotron Maser Instability mechanism (CMI) [*Wu and Lee,* 1979] have been proposed to explain the radiation of AKR; the R-X mode waves are generated directly through the cyclotron type resonance condition under the relativistic effect of the high energy electrons. On the other hand, the indirect mechanism of the Mode Conversion mechanism (MC) [*Oya,* 1971; 1974] has been also proposed; L-O mode waves are generated through the mode conversion process along the propagation path of plasma waves. Then, it is important to evaluate how these mechanisms work for the generation of DAMs on the basis of the identification of propagation modes of DAMs.

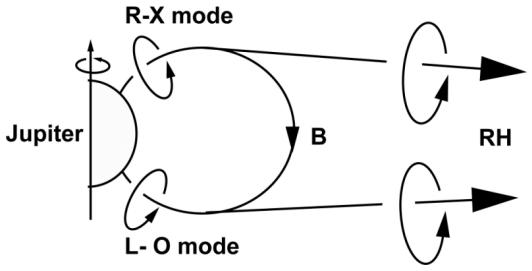

Figure 1. The relation between the source location and the observed polarization sense. When the RH emission is observed, the emission is generated in the form of R-X mode if the emission is from the northern hemisphere. On the other hand, the emission is generated in the form of L-O mode if the emission is from the southern hemisphere.

Main objective of the present interferometer observation system of DAMs is to identify the propagation mode of DAMs through the determination of the source location. In the case of usual observation from the ground, strong DAMs appear with dominant right handed (RH) polarization sense [*Barrow and Morrow,* 1968]. As shown in Figure 1, if RH emissions are radiated from the northern hemisphere, the emissions are generated in the propagation mode of the R-X mode at the sources, while if they are from the southern hemisphere, the emissions are generated in L-O mode waves. Many observational evidences suggest that DAMs are predominantly generated in R-X mode [*Zarka,* 1998]. Thus, it has been generally believed that the sources of DAMs are located mainly in the northern polar ionosphere. However, recent Jovian auroral images suggest that some parts of DAMs are possibly generated also in southern polar ionosphere, then, it is propagating with L-O mode through the MC mechanism.

From the viewpoint mentioned above, the interferometer observation has been carried out in the Tohoku University since early 1980's [*Tokumaru,* 1985]. Based on the previous works, an ionosphere effect is found to be a key term for the long baseline interferometer. There has been the major problem for the single frequency observation. In the single frequency observation, difference in the Total Electron Content (TEC) of the terrestrial ionosphere along the ray paths of each station affects directly the observed fringe phase. In order to compensate the influence of the ionosphere, we have developed the double frequency interferometer technique, which have been established in VLBI [*Murao,* 1995]. However, comparing with usual VLBI technique, the present DAM observation frequencies are much low and very close to

each other. Thus, precise evaluation of ionosphere effect is needed to find the validity of the double frequency interferometer system for DAMs.

2. Simulation

2.1 The key parameters of the observation

The simulation study on the double frequency interferometer system for DAM observations has been carried out for following points; (1) Whether the fringe phase signal can be obtained accurately enough to determine the source location. The accuracy of fringe phase is largely affected by the signal to noise (S/N) ratio of the DAM signal and by the product of the receiver bandwidth and the integration time. The required accuracy of the fringe phase is decided by the stability of the solution of the inverse problem. The baseline length and the interval of two observation frequencies are playing the important role at this point. (2) Whether the assumption of the ray paths used in the theory can be satisfied for the observation conditions. In general, the interferometer system requires that the ionosphere effects on each ray paths are correctable. However, due to the propagation property of the low frequency radio waves, it is necessary to evaluate the validity of the assumption that the difference of the ray paths for two observation frequencies is negligible small.

In this simulation, the parameters mentioned above are set to be the realistic values. In the interferometer system of Tohoku University, the baseline lengths are ranging from 44 to 116 km. The typical DAMs appear within a time range from a few minutes to a few hours and with frequency bandwidth from a few hundred kHz to a few MHz. The minimum fringe period is a few second in case of long baseline. Then, the baseline length, the observation frequencies, the receiver bandwidth, and the integration time are set to be 100 km, 22.0 MHz, 22.5 MHz, 10 kHz, and 0.2 second, respectively.

2.2 The procedure of simulation

The procedure of the simulation is derived into two stages: The first stage is the simulation of observation signals where the DAM signal is synthesized as a random noise feature, and added with background galaxy noise which is also generated as another random noise as described in subsection 2-3-1. In this stage, we also used the 2D ray-trace to calculate the fringe pattern under the given source location and the electron density distribution of terrestrial ionosphere. The second stage is the data analysis stage where the signals from the double frequency interferometer system are analyzed to determine the source location by solving the inverse problem. The validity of the double frequency interferometry is, then, evaluated by comparing the analyzed location with the given source location.

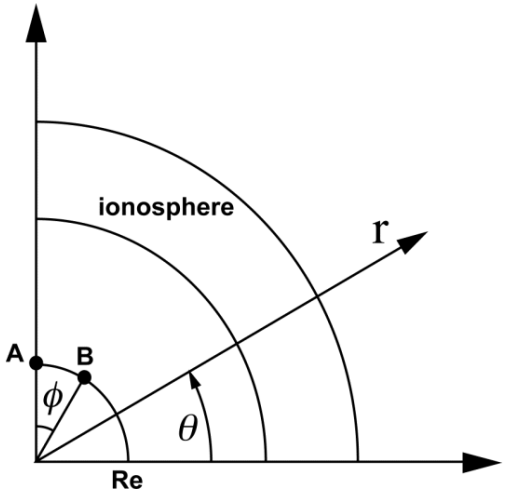

Figure 2. The 2D polar coordinate used in this simulation. A, B are the stations and Re is radius of the Earth. The angle Φ *is set to be approximately* 1.57×10^{-2} *radian so that the length of the baseline is 100 km.*

2.3 The observation stage

2.3.1 The synthesis of DAM signal models

This simulation is applied on the signals observed at two observation stations located in the two-dimensional polar coordinate as shown in Figure 2. In this stage, the models of frequency-converted DAM signals are synthesized as a random noise with frequency range from DC to 10 kHz. In the same manner, the background galaxy noise is also synthesized as another random noise, and added to the synthesized DAM signals. For generating a random noise signal, we used an analog to digital conversion of a noise generator signal. The observed time series data at A and B station, $P_a(t)$ and $P_b(t)$ are respectively expressed as

$$\begin{cases} P_a(t) &= S(t) + N_a(t) \\ P_b(t) &= S(t+\tau) + N_b(t) \end{cases} \quad (1)$$

where $S(t)$ is DAM signal, and $N_a(t)$ and $N_b(t)$ are galactic noise at A and B station. We can examine for arbitrary S/N ratio for the observed data to evaluate the effect of this S/N ratio on the source determination. The spectrum and auto-correlation function of a noise signal is shown in Figure 3. Thus, any noise signal has no correlation to others. The synthesized DAM signals which gives the

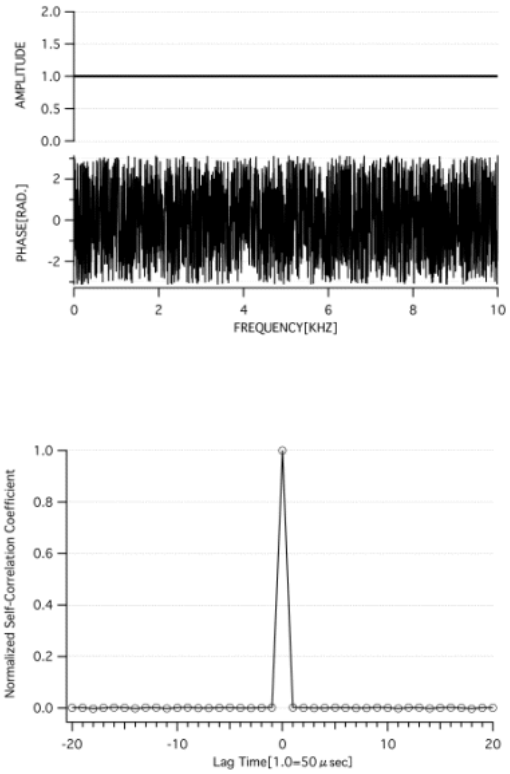

Figure 3. The spectrum (upper panel) and auto-correlation function (lower panel) of a random noise. After A/D conversion, the amplitude of the random noise is set to be same in each frequency component. The features are almost the same as the features of white noise.

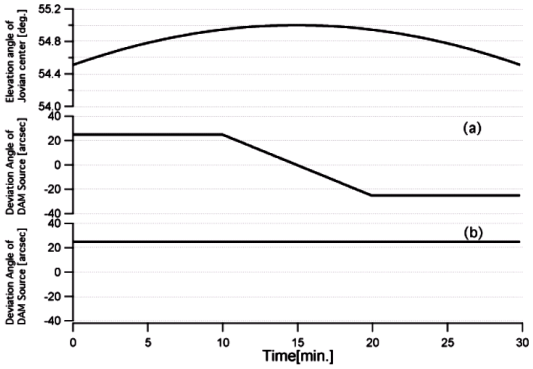

Figure 4. The given time series of source location. The elevation angle of Jovian center at station A is shown in the upper panel. The deviation angle of the given source from the Jovian center is shown in panel (a) and panel (b). In this simulation, the angular diameter of Jovian disc is set to be 50 arcsec. (a) The case that the source location changes from northern to southern hemisphere. (b) The case that the source location exists stationary at the northern hemisphere.

signals received at A and B stations has a correlation by using the delay time calculated by 2D ray-tracing as following section.

2.3.2 The 2D ray-tracing

The ray path trace of the observation signals is carried out under the two-dimensional polar coordinate as shown in Figure 2. As shown in Figure 4, the elevation angle of the Jovian center at station A varies within a range from 54.5 deg. to 55.0 deg. that corresponding with the actual variation of the height of Jovian center observed at Sendai in 2002. We used two cases of DAM source locations; one is a rapid change of DAM source from northern to southern auroral ionosphere of Jupiter. The other case is stable source location in the northern Jovian ionosphere.

The electron density distribution in the terrestrial ionosphere is assumed consisting of two components, i. e, the background stationary ionosphere profile expressed by spherical Chapman function and overlapping variable component expressed by the sine function corresponding to a disturbance of Traveling Ionospheric Disturbances (TIDs). The former component expresses mainly the density profile in F region because that the electrons in F region contribute largely to TECs. The peak density, the peak altitude of plasma density, and the scale height are 5.0×10^5[1/cc], 300 km, and 60 km, respectively. The latter variable component is given as

$$\delta N(r,\theta,t) = N(r)\varepsilon \exp\left[-\frac{1}{2}\left(\frac{r-R_e-z}{\sigma}\right)^2\right] \cdot \sin\left[2\pi\left(\frac{r\theta}{\lambda}-\frac{t}{T}\right)\right] \quad (2)$$

where $N(r)$ is the background stationary component, ε is the amplitude of TID 's, T is the period, λ is the wavelength, z is the altitude of center, and σ is the radial range. For the present calculation, T, λ, z, and σ are set to be 30 minutes, 100km, 300km, and 1000 km, respectively. By using these values for parameters in the simulation, the theoretical delay time is computed by the 2D ray-tracing analysis and used for giving a correlation between the models of DAM signals which express the signals received at A and B stations.

2.4 The data analysis stage

The data analysis stage consists of the correlation process stage and the inverse problem stage. In the correlation process stage, the observed signals are transformed to Fourier components. The

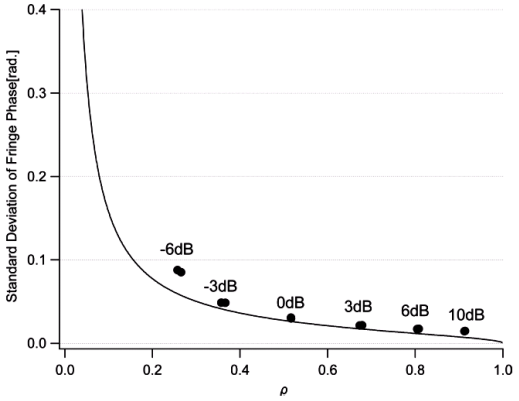

Figure 5. The relation between S/N ratio and standard deviation of fringe phase in the case that bandwidth is 10kHz and the integration time is 0.2second. ρ *is defined by equation (4). A solid line shows the theoretical expectation (equation (3)) and the points show the result calculated in this simulation. The values in decibel in the figure show S/N ratio set initially. The results obtained in this simulation are consistent with the theoretical expectations.*

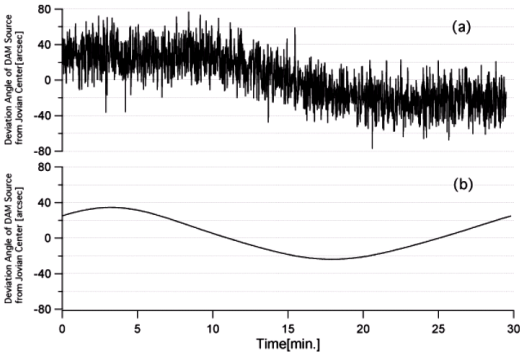

Figure 6. The deviation angle of the obtained source location from Jovian center. (a) The case that no TIDs exists considering only the effect of S/N ratio. In this case, the given source location moves from northern to southern hemisphere as shown in Figure 4. (a). The movement of the source from north to south is roughly obtained. (b) The case that no galaxy noise exists considering only the effect of TIDs. In this case, the given source location is stationary at the northern hemisphere as shown in Figure 4. (b). But, the obtained source location moves from north to south.

normalized cross-correlation coefficients are calculated in frequency space; the integration is carried out after subtracting the fringe phase corresponding to the center of Jovian disc. Figure 5 shows the relation between the S/N ratio and the standard deviation of fringe phase pattern. The standard deviations obtained in this simulation are consistent with the theoretical values given by

$$\sigma = \sqrt{\frac{1}{2BT}\left(\frac{1}{\rho^2} - 1\right)} \tag{3}$$

where σ, B, T is the standard deviation of fringe phase, the bandwidth, the integration time, respectively. The value of σ is given as follows

$$\rho = \sqrt{\frac{T_{as}T_{bs}}{(T_{as}+T_{an})(T_{bs}+T_{bn})}} \tag{4}$$

where T is the equivalent noise temperature (a, b indicate the A, B station, and s, n indicate signal, noise, respectively) [*Takahashi et al.,* 1997]. In this simulation, T_{as}/T_{an} and T_{bs}/T_{bn} give the S/N ratios of signals. From Figure 5, the standard deviation of fringe phase can be obtained for the S/N ratio of the signals.

In the inverse problem stage, a matrix equation is solved to determine the source location. In the simulation, fringe rate is used in the calculations instead of absolute value of fringe phase because the absolute value of fringe phase is difficult to be determined in the present interferometer observations. This means that only the relative motion of source location can be obtained by solving the present inverse problem. In Figure 6, examples of results for the case of low S/N ratio in the observation (panel (a)) and large amplitude TIDs (panel (b)), analyzed source locations are shown. In the panel (a), the simulation is carried out for low S/N signals without effect of TIDs. In this case, the movement of the source representing the switching phenomena of the source position as shown in Figure 4. (a) has been used for the fringe phase calculation. Even though the low S/N ratio set as -6 dB, the fringe phase is reproduced within 0.1rad of the standard deviation (see Figure 5). The movement of the source from northern to southern hemisphere is detectable for the present observation parameters. In the case (b), the simulation is carried out considering only the effect of TIDs and excluding the effect of background galaxy noise. In this case, source location is fixed in the northern hemisphere as shown in Figure 4. (b) and the time variation of the difference in TEC between A and B stations is assumed as $1.0\times10^{16}[1/\mathrm{m}^2]$. The obtained source location moves from northern to southern hemisphere even for the given stationary source location at the northern hemisphere. The apparent movement of the source location is caused by the difference of ray paths between two observation frequencies. Considering these results, we can determine the source position with enough accuracy ($\delta\theta \leq 25$ arcsec) for the case when the fringe phase

is measured with standard deviation less than 0.1 radian, and the limit of TEC variation is evaluated to be less than $5.0\times10^{15}[1/\mathrm{m}^2]$.

3. Discussion and conclusion

Based on the simulation study, it is concluded that the double frequency interferometer method for the long baseline interferometer can be applied for DAM signals under the following condition; (1) The fringe phase is determined with standard deviation less than 0.1 radian which is corresponding to the case when the S/N ratio in the observation is above -6 dB, for the receiver bandwidth and the integration time of 10 kHz, 0.2 second, respectively. (2) The limit of variation of differential TEC between A and B stations should be less than about $5.0\times10^{15}[1/\mathrm{m}^2]$ during the typical observation time interval of DAMs.

In Tohoku University, a new interferometer system is planned on the basis of the double frequency interferometry discussed in this paper. The bandwidth of receivers is set to be 10 kHz, and the phase stability is set to be less than about 0.1 radian. The result of the present simulation study confirms the validity of the new interferometer system for the DAM observation with limit of the S/N ratio above about -6 dB.

From the GPS observations, it has been shown that the amplitude of TIDs is often increased as large as $10^{16}[1/\mathrm{m}^2]$ in Japan [*Saito et al.,* 1998]. In that case, the TID magnitude is judged as larger than the limit. However, based on the continuous monitoring of the TEC data above the observation stations, it becomes possible to judge the validity of the long baseline interferometer observations.

References

Barrow, C. H., and D. P. Morrow, The polarization of the Jupiter radiation at 18 Mc/s, *Astrophys. J.*, 152, 593-608, 1968.

Broadfoot, A. L., M. J. S. Belton, P. Z. Takacs, B. R. Sandel, D. E. Shemansky, J. B. Holdberg, J. M. Ajello, S. K. Atreya, T. M. Donahue, H. W. Moos, J. L. Beataux, J. E. Blamont, D. F. Strobel, J. C. McConnell, A. Dalgarno, R. Goody, and M. B. McElroy, Extreme ultraviolet observations from Voyager 1 encounter with Jupiter, *Science*, 204, 979-982, 1979.

Murao, H., Identification of the Jovian Decameter Wave Radiation Sources Using Two-Frequency Interferometer Network System, Ph.D. thesis, Tohoku Univ., 1995.

Oya, H., Conversion of electrostatic plasma waves into electromagnetic waves: Numerical calculation of the dispersion relation for all wavelengths, *Radio Sci.*, 6, 1,131-1,141, 1971.

Oya, H., Origin of Jovian decameter wave emissions-conversion from the electron cyclotron plasma wave to the ordinary mode electromagnetic wave, *Planet. Space. Sci.*, 22, 687-708, 1974.

Saito, A., S. Fukao, and S. Miyazaki, High resolution mapping of TEC perturbations with the GSI GPS network over Japan, *Geophys. Res, Lett.*, 25, 3,079-3,082, 1998.

Takahashi, F., T. Kondo, and Y. Takahashi, "Very Long Baseline Interferometer" (in Japanese), pp.104-107, Ohm Co., Ltd., Tokyo, 1997.

Tokumaru, M., Studies on the location of Jovian decametric radiation using 1 km and 75 km interferometers, Ph.D. thesis, Tohoku Univ., 1985

Wu, C. S., and L. C. Lee, A theory of the terrestrial kilometric radiation, *Astrophys. J.*, 230, 621-626, 1979.

Zarka, P., Auroral radio emissions at the outer planets: Observations and theories, *J. Geophys. Res.*, 103, 20,159-20,194, 1998.

High-sensitivity astronomical observation with GALAXY

Kenta Fujisawa[1] (*kenta@hotaka.mtk.nao.ac.jp*), **Noriyuki Kawaguchi**[1], **Hideyuki Kobayashi**[1], **Tetsuro Kondo**[2], **Junichi Nakajima**[2], **Hisashi Hirabayashi**[3], **and Yasuhiro Murata**[3]

[1] *National Astronomical Observatory of Japan (NAO)*
Osawa 2-21-1, Mitaka, Tokyo 181-8588, Japan
[2] *Kashima Space Research Center*
Communications Research Laboratory
893-1 Hirai, Kashima, Ibaraki 314-0012, Japan
[3] *Institute of Space and Astronautical Science (ISAS)*
Yoshinodai 3-1-1, Sagamihara, Kanagawa 229-8510, Japan

1. Introduction

GALAXY is a research project on advanced VLBI technology, jointly conducted by CRL, NAO, and NTT. The testbed of the project is a 2.5-Gb/s ultra-high speed network using Asynchronous Transfer Mode (ATM). One of the aims of this project is to achieve high-sensitivity VLBI observation with this gigabit network [1].

The GALAXY observations have been carried out since 1998 using conventional VLBI terminal of 256-Mb/s developed for KSP [2]. Here we report the recent results of GALAXY observations with new 1-Gb/s system. Developments of new networking technology such as Internet Protocol (IP) with the GALAXY network are also presented in the section 3.

2. 1-Gbps observation system

Figure 1 shows the 1-Gb/s (1024-Mb/s) observation system, the participating telescopes are Usuda 64m (ISAS) in Nagano and Kashima 34m (CRL) in Ibaraki connected by GALAXY network provided by NTT. The gigabit sampler and the correlator have been developed by CRL for tape-based system [3], and the VLBI/ATM interface was developed by NAO. The data stream of Usuda 64m are ATM celled and transmitted to Kashima. The received ATM cells are retrieved as VLBI data stream at Kashima and correlated with the data of 34m telescope in real-time.

The first experimental observation with this 1-Gb/s system was made on June 23, 2001. Before starting the observation, a network delay was measured. This is for compensation of unpredictable delay caused by digital network.

The observing frequency was 8080-8592 MHz with lack of lower 100 MHz (8080-8180 MHz) due to the analogue bandbass character. The observed sources are 3C273, 3C279, NRAO530, and Sgr A*, which are strong enough for experimental fringe detection. As the result, strong fringes were successfully detected in real-time (Figure 2). The fringe phase and amplitude were stable during the observation for 7 hours. The detection sensitivity and brightness sensitivity derived from the Signal-to-Noise ratio are about 2-mJy and 4×10^4K respectively with 600 sec integration.

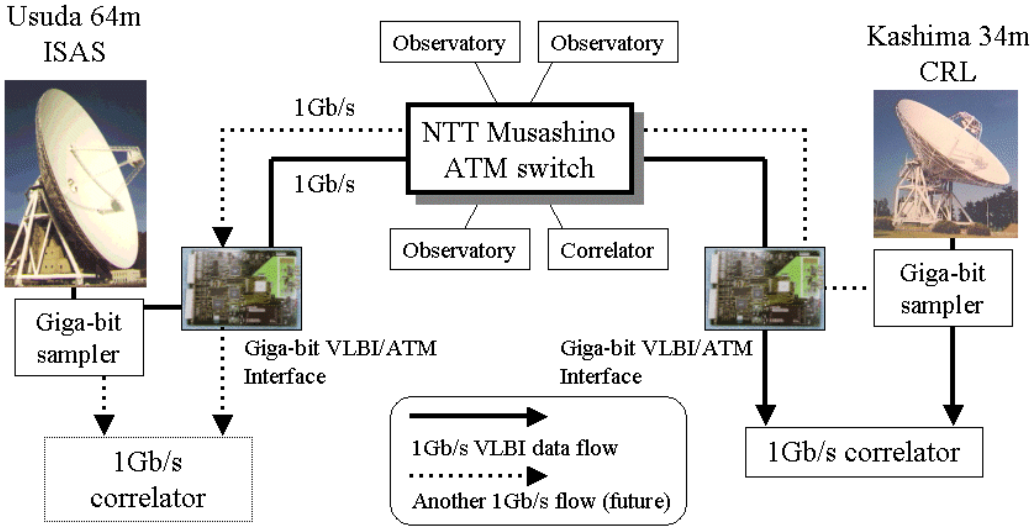

Figure 1. The network of 1-Gb/s experimet. The VLBI data sampled at Usuda are transmitted to Kashima and correlated with the data sampled at Kashima.

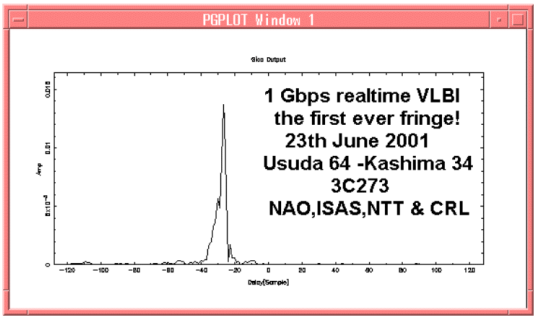

Figure 2. 1-Gb/s real-time the first ever fringe between Usuda and Kashima on June 23, 2001. The source is 3C273.

The successive astronomical observations have been carried out with this 1-Gb/s system since Oct 29, 2001. According to the preliminary analysis, a source with total flux density of 3 mJy was detected. This result demonstrates that GALAXY does have capability for detecting weak radio sources.

3. Future Plan

At present, GALAXY is using ATM for the network transmission system. The explosive spread of the Internet, however, is making Internet Protocol (IP) a major data transmission protocol. A research and development of IP transfer technique for high-speed VLBI data, and improvement of connectivity with a number of other research observatories are undergoing using GALAXY network. These activities are reported in this issue by Kondo and by Iwamura, respectively.

The current 1-Gb/s observation system consists of single baseline. At least three baselines are required to obtain a closure phase for astronomical study of radio source structure. Such multi-baseline observation will be realized with the ‘ distributed-gigabit network interface ’ and the ‘ distributed-gigabit correlator ’those are under development in National Astronomical Observatory of Japan. These equipments are designed suitable for network-type VLBI observation. This new system will have observation capability of 2-Gb/s VLBI data for 3-baselines. Moreover, a 4-Gb/s observation could be achieved using full-duplex network capability. This ultra-wideband system will make GALAXY as a unique VLBI network in the world (Figure 3), and let us observe thermal objects with low brightness temperature of a few tens of thousand Kelvin.

Acknowledgement: The authors would like to thank all members of GALAXY team of CRL, NAO, ISAS and NTT.

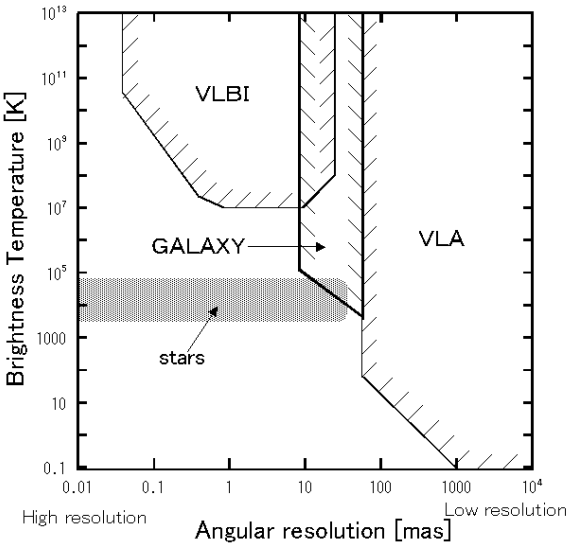

Figure 3. Angular resolution and brightness sensitivity. The mild resolution and high-sensitivity of GALAXY make it a unique network for detecting small and low brightness radio sources, such as stars.

References

[1] Kenta Fujisawa, Noriyuki Kawaguchi, Hideyuki Kobayashi, Satoru Iguchi, Takeshi Miyaji, Kazuo Sorai, Tetsuro Kondo , Yasuhiro Koyama, Junichi Nakajima, Mamoru Sekido, Hiro Osaki, Hiroshi Okubo, Hitoshi Kiuchi, Yukio Takahashi, Akihiro Kaneko, Hisashi Hirabayashi, Yasuhiro Murata, Hisao Uose , Sotetsu Iwamura, and Takashi Hoshino, “GALAXY — Real-time VLBI for Radio Astronomy Observations ”, Journal of the Communications Research Laboratory, Vol.46, No.1, pp.47-58, March 2001

[2] Hitoshi Kiuchi, Tetsuro Kondo, Mamoru Sekido, Yasuhiro Koyama, Michito Imae, Takashi Hoshino, and Hisao Uose, “Real-Time VLBI Data Transfer and Correlation System”, Journal of the Communication Research Laboratory, Vol.46, No.1, pp83-89, March 1999

[3] Nakajima J., Koyama Y., Sekido M., Kurihara N., Kondo T., Kimura M., Kawaguchi N., “ 1-Gb/s VLBI, the first detection of fringes ” Experimental Astronomy, Vol.11, pp.57-69, 2001

NTT's Ultra High-speed Network Experiment and Realtime VLBI Trials

Hisao Uose[1] (*uose.hisao@lab.ntt.co.jp*), **Sotesu Iwamura**[1], **and Takashi Hoshino**[2]

[1] *NTT Information Sharing Platform Laboratories*
3-9-11 Midori-cho, Musasino-shi,
Tokyo 180-8585, Japan
[2] *NTT Advanced Technology*
549-2 Shinano-cho, Totsuka-ku, Yokohama-shi
Kanagawa 244-0801, Japan

1. Introduction

In 1995, NTT Laboratories have started a joint research project on ultra high-speed communications with public research organizations using a large scale network testbed having the maximum speed of 2.4 Gb/s. Among many applications tried in the first phase of the project, the realtime VLBI (very long baseline interferometry) has proved to be benefited greatly from the high performance communications technologies. With the realtime data transmission using high-speed communications network, the bottleneck regarding the data transfer in the conventional VLBI system can be removed. Furthermore, as the bandwidths of the network become larger, the performance of the observation system will become better.

In the second phase of the project started in 1998, therefore, the focus is placed on the advancement of this real-time VLBI technology. Extensive research items regarding the realtime VLBI technology are being conducted, together with the scientific observations using the testbed. So far, through the experiments using the developed realtime VLBI system, great improvement in observation performance has been achieved. This paper explains the outline of this research project from the viewpoint of communications technologies which play a major role in the realtime VLBI system.

2. Realtime VLBI trial in the framework of NTT's "Very high speed network experiment"

NTT Laboratories have started a joint research project on very high speed networking with public research institutes including Communications Research Laboratory (CRL), National Astronomical Observatory (NAO) and Institute of Space and Astronautical Science (ISAS) in June 1995. The purposes of the projects at NTT side were twofold. One is to establish technologies for very high-speed communications (Gb/s class for each application) preparing for the very high speed communications services in the future. The second aim is to explore and prove the effectiveness of

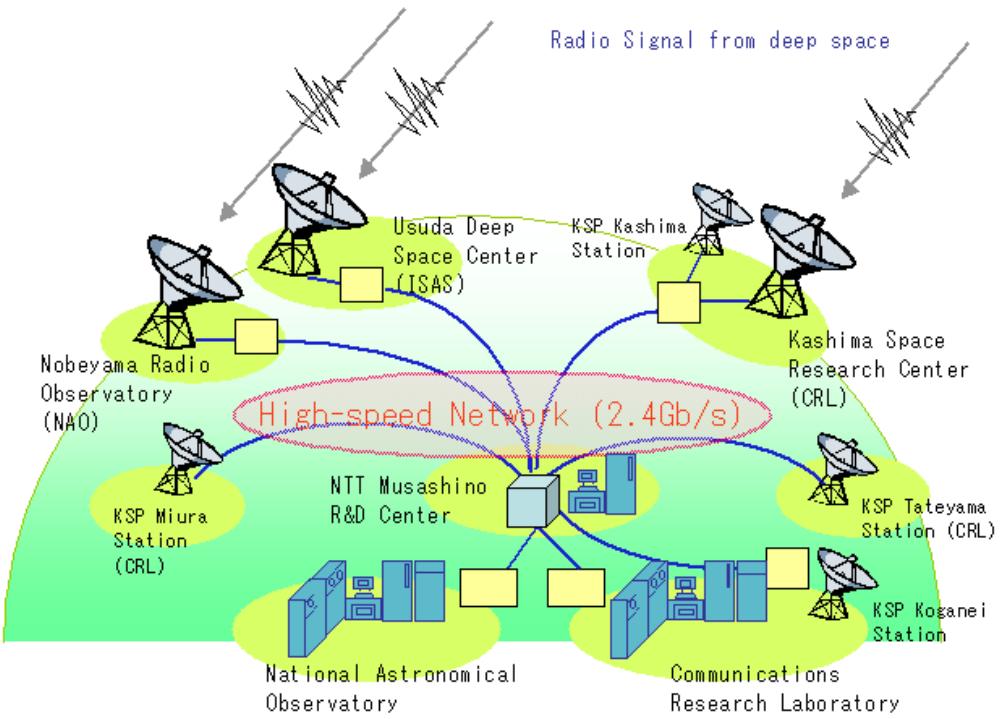

Figure 1. Realtime VLBI testbed.

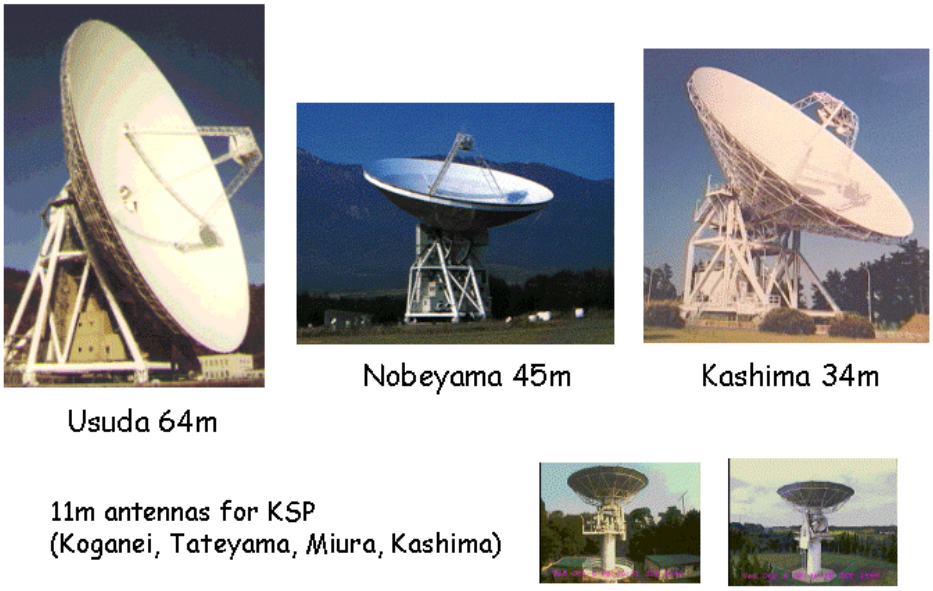

Figure 2. Antennas used for experiments.

those technologies in advanced scientific areas which seemed to be the first applications of this kind utilizing the vast capabilities of high-speed communications technologies.

With the belief that the joint effort with the applications users, in this case, VLBI researchers is indispensable for a fruitful achievement, we have constructed a dedicated ATM network spanning Kanto/Shinetsu area and provided the facilities to our research partners together with the necessary technologies to adapt their equipment to connect to the experimental network. The network connected the NTT R&D centers and participating research organizations with 2.4 Gb/s circuits, repeaters, ATM Switches and high-performance IP routers. We have also connected six antennas as shown in the Figure 1 for our trials. Figure 2 shows the pictures of those antennas and Figure 3 shows an example of " fringes " obtained with this experimental system.

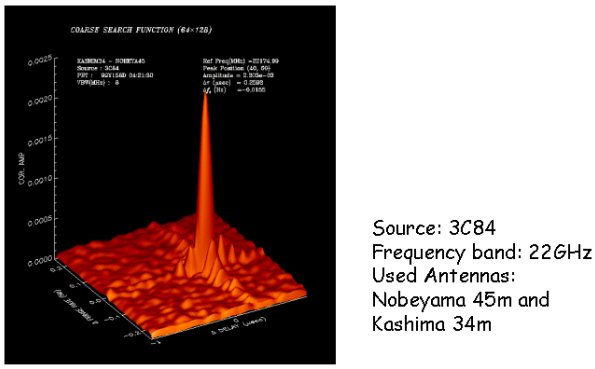

Figure 3. Example of Correlated Data.

3. Realtime VLBI Applications

With the conventional tape-based VLBI system, the amount of observation data was restricted by the data rate and storage capacity of the data recorder used to store observed radio signals at each antenna site, limiting the performance of the total observation system. With the realtime VLBI system directly connecting antennas and data processing units with communications network, however, this restriction can be removed and the larger amount of data can be utilized for analyses. Thus, the total performance of the VLBI system is only limited by the performances of observation system (antennas, receivers and samplers, etc.) and processing units (cross correlators). In addition, realtime cross correlation during the observation is made possible allowing researchers to check the status of their observation at the spot. Consequently, realtime VLBI brings great advantages over the conventional tape-based system in both aspects of system performance and observation flexibility and efficiency. We have two applications using the realtime VLBI in our project, geodesy and radio astronomy.

3.1 Geodesy (KSP Project)

This is a joint trial with CRL to implement a high precision crustal deformation measurement system using realtime VLBI. CRL has constructed four dedicated antennas shown in Figure 4 for this project called KSP (Key Stone Project). By connecting those antennas with the central cross cor-

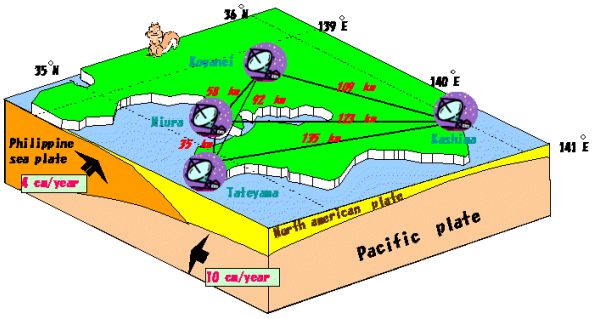

Figure 4. Location of KSP measurement sites.

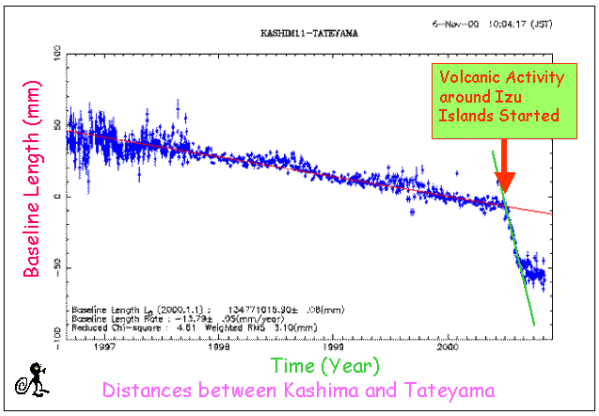

Figure 5. Distance fluctuations observed in KSP.

relator located in CRL Koganei, Tokyo, measurements with very high resolutions have been made possible. The net data rate from each antenna is 256Mb/s and the signals are routed to Koganei through NTT Musashino Research and Development Center. With this measurement system, the deformation in Kanto (larger metropolitan Tokyo) area can be measured with the precision of millimeters.

Since 1996, regular measurements are being conducted using the KSP network and the large amount of observed data is publicly offered to earth science community through the CRL web site. Figure 5 shows the measured distances between Kashima and Tateyama using this system. A major deformation due to a sudden volcanic activity around Izu Island can be observed at the right hand side of the figure.

3.2 Radio astronomy (GALAXY Project)

This is a joint effort with NAO, CRL and ISAS to implement the world 's largest virtual radio telescope having ultra-high resolution/sensitivity by combining conventional VLBI technology and the newest Gb/s class communications network. By adopting the VLBI technology, a large virtual telescope can be constructed with multiple antennas.

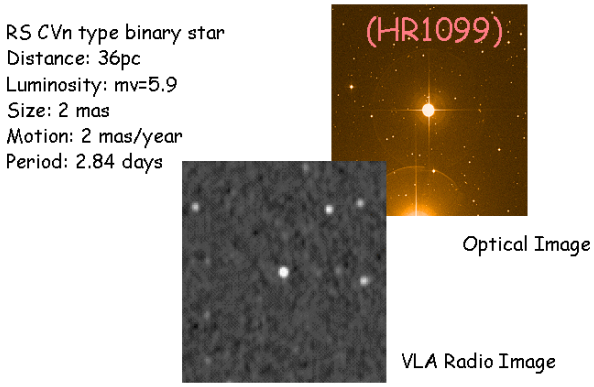

Figure 6. Observation of Bursty Radio Source.

The synthesized virtual telescope has the same angular resolution of one very large telescope with the diameter which is equal to the distance between the remote antennas, in the case of Kashima-Usuda baseline, 208km.

The on-site processing/observation brought by the realtime VLBI has allowed us to conduct very flexible and efficient VLBI observations, by constantly checking the obtained data while we are tracking the target radio source. This is only possible with the realtime VLBI technology. We can use antennas shown in Figure 2 together with a space radio telescope HALCA using our network. The first fringe (cross correlation) was detected in 1997 between the signals received by a terrestrial antenna (Usuda) and a satellite antenna (HALCA). Realtime correlation has been successfully established among large terrestrial antennas (Usuda, Nobeyama and Kashima) in 1998. Figure 6 shows an example of observation which proved the effectiveness of the realtime VLBI. This observation of this bursty radio source was possible by catching a sudden variation of signal strength during the realtime observation.

4. Networking issues

4.1 Internet VLBI and distributed computing

In the first phase of the project, we used ATM (Asynchronous Transfer Mode) technology to carry radio signals. The ATM technology has the precise bandwidth management capabilities enabling a very stable transmission required for the critical applications like realtime VLBI. In the second phase, however, we started to study to utilize IP (Internet Protocol) technologies extensively within our experimental network together with ATM.

To make the realtime VLBI experiment more affordable and widespread, the use of IP technologies will be effective, because research and edu-

cation networks around the world are rapidly increasing their capacities and those networks are accessible from public research organizations around the world. Standing on this viewpoint, we are developing very high speed IP technology applicable to realtime VLBI system. This involves challenging research issues including high speed IP stream transmission and advanced network resource management. In addition, we've started the research on distributed processing using a number of PCs connected by high performance network for calculating cross correlation of the radio signals. This approach is in line with other similar effort best represented by the GRID project.

4.2 Adoption of photonic technologies

NTT Laboratories have a large R&D force in the field of photonic networking technologies. We've just started to cooperate with them to further strengthen the infrastructure of our network testbed. Now the new pieces of WDM (Wavelength Division Multiplexing) equipment are being deployed in our network with an innovative AWG device developed at our laboratories. This will allow us to use more bandwidth for the future experiments.

5. Conclusions

In June this year, we have successfully achieved the first realtime VLBI observation with the processing speed of 1Gbps in the world, using the 64m antenna of Usuda Deep Space Center and the 34m antenna of CRL Kashima Space Research Center. This achievement has a great significance opening up a new vista in the field of VLBI radio astronomy by improving the detection sensitivity of the observation system. The detection of the very weak radio sources will also accelerate the study to construct space-time standard infrastructure in space, which is being conducted at CRL including the real-time and high time-resolution determination of the earth orientation parameters.

We plan to further improve the detection sensitivity of the real-time VLBI observation system by raising the transmission/processing speeds up to 2Gb/s next year in parallel with the upgrading of the experimental network. The development of " Internet VLBI "systems and the distributed cross-correlation system using the networked computers are other targets. The cooperation with research institutes abroad is also being sought to realize an international realtime VLBI observation system.

References

[1] GALAXY team: "Ultra High-speed Network Experiment, " NTT R&D Special Issue, Vol.50, No.10, pp.792-857, 2001 (in Japanese).

[2] H. Kiuchi, M. Imae, T. Kondo, M. Sekido, S. Hama, T. Hoshino, H. Uose and T. Yamamoto,, "Real-Time VLBI System Using ATM Network, " IEEE Trans. on Geoscience and remote sensing, Vol. 38, No.3 , 2000.

[3] P.J. Diamond, "The MERLIN upgrade, " Proceedings of SPIE Vol. 4015, 2000.

A Study on VLBI Data Transfer Using IP

Sotetsu IWAMURA[1] (*si@seven.nal.ecl.net*), **Hisao UOSE**[1], **Tetsuro KONDO**[2], **Shin-ichi NAKAGAWA**[3], **and Kenta FUJISAWA**[4]

[1] *NTT Information Sharing Platform Laboratories*
3-9-11 Midori-cho, Musasino, Tokyo
180-8585, Japan
[2] *Kashima Space Research Center*
Communications Research Laboratory
893-1 Hirai, Kashima, Ibaraki 314-0012, Japan
[3] *Communications Research Laboratory*
4-2-1 Nukui-kita, Koganei, Tokyo 184-8795, Japan
[4] *National Astronomical Observatory of Japan*
2-21-1 Osawa, Mitaka, Tokyo 181-8588, Japan

1. Introduction

This paper presents our data transfer system for very long baseline interferometry (VLBI) using Internet protocol (IP). Since 1998, GALAXY project, which is composed of Communications Research Laboratory, National Astronomical Observatory of Japan, The Institute of Space and Astronautical Science and NTT, has been conducting experiments on real-time VLBI. In the experiments, observation data is transmitted over NTT's 2.4 Mbps asynchronous transfer mode (ATM) network; therefore, we can catch up with real-time phenomena as well as improve observation efficiency. In addition to the experiments based on ATM, we have been focusing on IP transfer for VLBI data delivery. Adopting IP technique into real-time VLBI brings the following advantages that are essential to our goal.

- Improvement of interconnectivity with other observation sites far apart
- Easiness to introduce distributed processing schemes
- Utilization of low-cost but high-performance equipment

2. IP Transfer Architecture for Real-time VLBI

Figure 1 shows our current processing flow of VLBI observation data. A very weak signal from the space received with an antenna is converted into multi-channeled and time-stamped digital

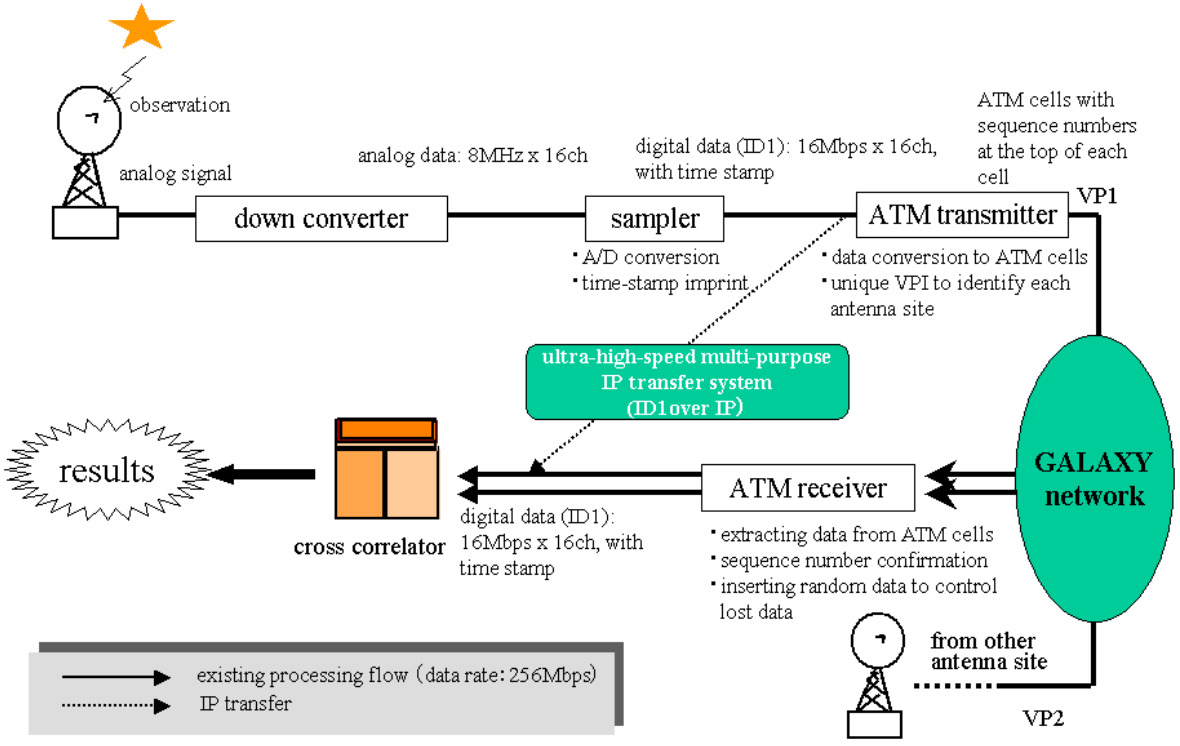

Figure 1. VLBI data processing flow in GALAXY project

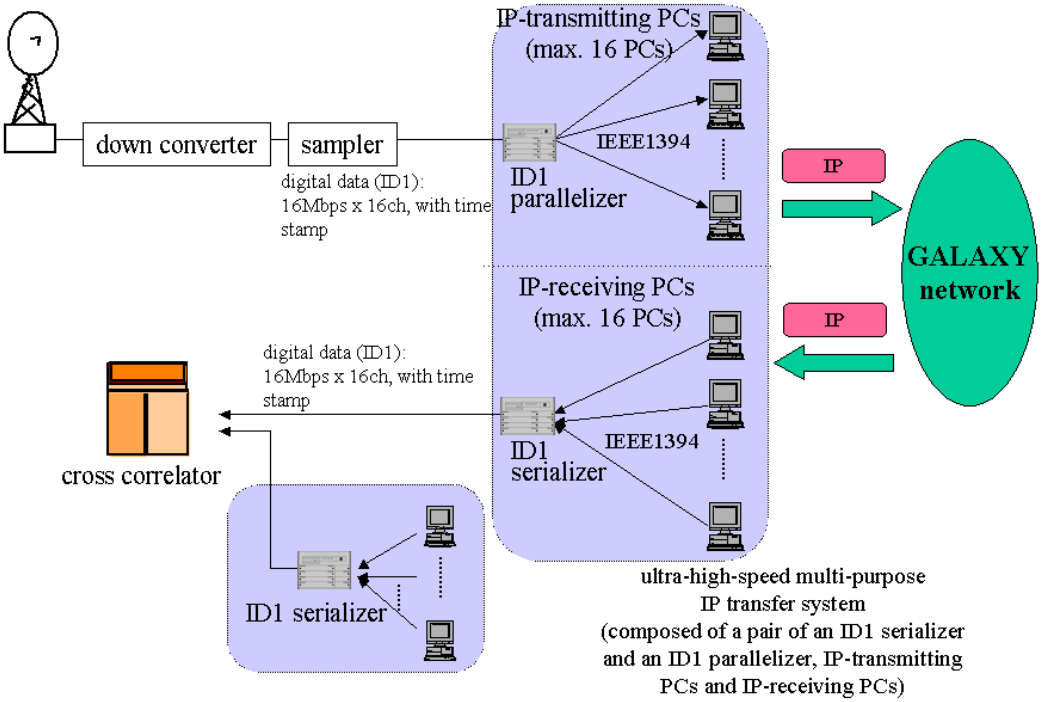

Figure 2. VLBI data transfer with ultra-high-speed multi-purpose IP transfer system

data and transmitted with an ATM transmitter in ATM cells. An ATM receiver extracts data from received ATM cells and sends it to a cross correlator. The cross correlator receives data also from other ATM transmitter and conduct cross-correlation processing. As our policies in achieving an IP transfer system, we have been focusing on the following points:

- Making the most use of the existing equipment such as the sampler and the cross correlator,
- Achievement of transparency in data transfer, and
- Examining performance of multi-purpose PC in IP transfer for real-time VLBI.

A dotted arrowed-line in Figure 1 means another path that our ultra-high-speed multi-purpose IP transfer system (referred as IP transfer system in the rest of this paper) provides. A configuration of the IP transfer system is shown in Figure 2. The system consists of an ID1 parallelizer, an ID1 serializer, IP-transmitting PCs, and IP-receiving PCs. Considering that data rate of the existing real-time VLBI observation is typically 256 Mbps, a parallel IP transfer schemes is required to use multi-purpose PCs. In the system, the ID1 parallelizer receives data stream from the sampler through the ID1 interface, and divides it into multiple IEEE1394 streams. Each IP-transmitting PC receives the IEEE 1394 stream, extracts observation data, and transmits it in IP packets. On receiving the IP packets, each IP-receiving PC extracts observed data and transfers it to the ID1 serializer in an IEEE 1394 stream. By receiving the IEEE 1394 data steams from the IP-receiving PCs, the ID1 serializer constructs the observation data and sends it to the cross correlator. Thus the cross correlator can process cross-correlating calculation, also by receiving other observation data from the other IP transfer system.

3. ID1 parallelizer and ID1 serializer

Internal action of ID1 parallelizer and ID1 serializer is shown in Figure 3. An ID1 parallelizer divides received data into multiple blocks of a fixed length and stores each of them in the internal queues, by a round robin manner. Accordingly, the top data blocks of each queue are transmitted in parallel IEEE 1394 streams. An ID1 serializer collects data blocks of the fixed length via IEEE 1394 interfaces. After receiving enough numbers of the data blocks, the ID1 serializer constructs observation data, also by adopting the same round robin scheme as the ID1 parallelizer 's, and outputs it through the ID1 interface.

4. IP-transmitting PC and IP-receiving PC

Each IP-transmitting PC receives data in an IEEE 1394 data stream, and transmits it in

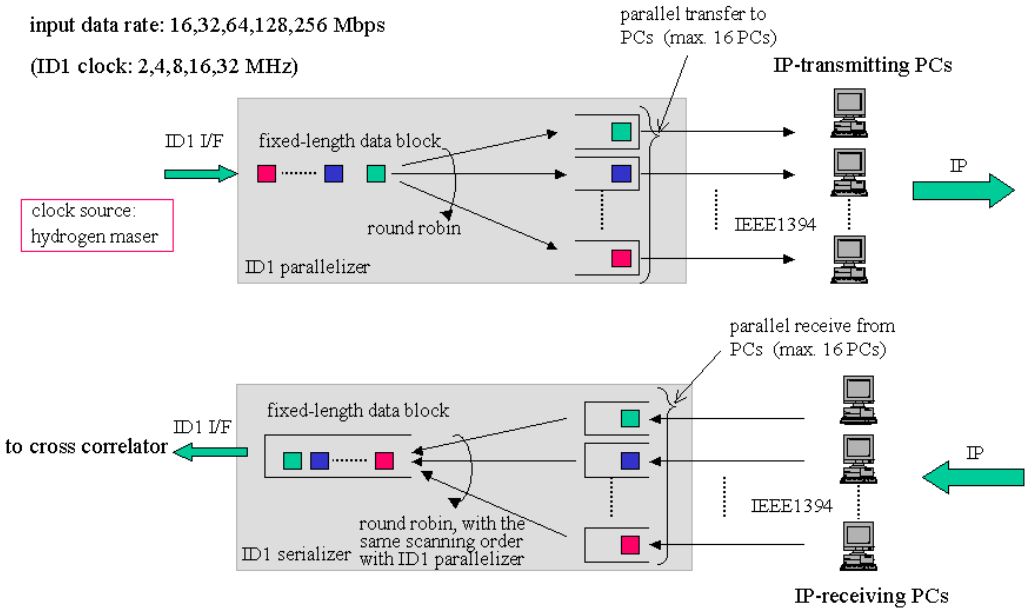

Figure 3. Internal action of ID1 parallelizer and ID1 serializer

Table 1. Major specifications of ID1 parallelizer and ID1 serializer

	ID1 parallelizer	ID1 serializer
Input I/F	ID1 x1	IEEE1394 x16
Output I/F	IEEE1394 x16	ID1 x1
Maximum PCs to connect	16	16
Internal data-block size (KB)	32, 64, 128, 256, 512, 1024 (manually selected)	←
ID1 clock (MHz)	Automatic synchronization to input ID1 I/F	2, 4, 8, 16, 32 (manually selected)
Maximum throughput (Mbps)	256	256

UDP/IP packets to the corresponding IP-receiving PC. The IP-receiving PC extracts data from received UDP/IP packets, and sends it in an IEEE 1394 stream. Accordingly, multiple UDP sessions are set up between the IP-transmitting PCs and the IP-receiving PCs. The reason we use UDP instead of TCP is to reduce PC's CPU load and not to be influenced by round trip time. Generally, parallel transfer scheme must guarantee data to correctly be ordered. In this system, by the round robin manner common both in the ID1 parallelizer and the ID1 serializer, the same data can be obtained from the ID1 serializer as the input data to the ID1 parallelizer. Another important issue to consider is possibility of packet loss, caused by lacking of retransmission mechanism on UDP. This can disturb the construction of correct data in ID1 serializer. In order to solve this problem, we have decided to generate random data of the same size on the IP-receiving PC when packet loss is detected. Detection of packet loss on receipt can be easily achieved by adding a sequence number at the top of each payload of UDP packets before transfer. This simple handling will cause no problem for cross correlation because result of cross correlation will little be influenced by inserting at most 0.1% of dummy data instead of correct ones.

5. Current Status

We have implemented ID1 parallelizers and ID1 serializers. Table 1 shows major specifications. Appearances of an ID1 serializer and an ID1 parallelizer are also presented in Figure 4. For IP -transmitting and -receiving PCs, we use Pentium2/400 PCs, on which Linux 2.4.6 is running. We confirmed ID1 throughput of 32 Mbps under the configuration described below.

- IP-transmitting PC: a PC with two IEEE 1394 interfaces, one 100BaseT interface

Figure 4. Appearances of ID1 parallelizer and ID1 serializer

- IP-receiving PC: a PC with two IEEE 1394 interfaces, one 100 BaseT interface
- IP network: both PCs are connected with a switching hub
- Protocol: a simple UDP transmission with no sequence numbers added on the IP-transmitting PC
- Input ID1 data to an ID1 parallelizer: generated with a test pattern generator (with an ID1 converter)
- Output ID1 data from an ID1 serializer: compared with the ID1 data generated in the test pattern generator

6. Conclusions and Future Plans

We have shown VLBI data transfer system using IP. We have as well described our successful experiment of ID1 data transfer at 32 Mbps, under the minimum configuration. We are currently working on the following issues.

- Transferring real VLBI observation data
- Implementing appropriate protocol between IP-transmitting PC and IP-receiving PC, which can adapt to dynamic change of network quality
- Improve performance

Parallel Data Processing System

Hitoshi KIUCHI(*kiuchi@crl.go.jp*)

Communications Research Laboratory
4-2-1 Nukui-kita, Koganei, Tokyo 184-8795, Japan

Abstract: In VLBI, the use of wide-bandwidth data generates a large SNR, proportional to $\sqrt{2BT}$ (B: bandwidth; T: integration time). Wide-bandwidth data acquisition is needed to enable sufficient sensitivity for measuring very small flux densities of cosmic radio sources in astronomical applications and high accuracy in geodetic applications. The GICO is the first giga-bit system, which has been used in astronomy and geodesy since 1999. However, even if wide-bandwidth high-speed processing are achieved, coherence deterioration remains a problem. In response to this situation, I developed new parallel processing method for wide-bandwidth high-speed data processing for the MVL (multi-media virtual laboratory) project. Our parallel processing system consists of a high-speed sampler, an ATM-interface unit, and a parallel-processing correlator.

1. High-speed sampler

The high-speed sampler is based on a commercially available digital oscilloscope (Tektronix TDS784). The development of this radio astronomical A/D sampler began in 1995. The oscilloscope has four analog-to-digital sampler chips operating at a maximum speed of 1 Gbps with a quantization level of eight bits for each sample. Two MSBs quantization bits of each sample (ch) are extracted from the digital oscilloscope and connected to the ATM-interface unit. A block diagram of the giga-bit sampler is shown in Fig. 1. The sampling rate was increased by 25.6/25, so that the original 1-Gsps sampler worked as a 1.024-Gsps sampler. We used sample rates ranging from 256 to 1024 Msps in 1- and 2-bit quantization.

The modification was done in the A/D sampled-signal pick-up daughter part installed in the oscilloscope. The output signal is sent via a high-speed parallel coax and the (4-channel) * (256 or 512 or 1024 Msps) * (2-bit sampling) data are output from the pick-up daughter part.

1.1 Signal-path compensation (self-calibration)

The oscilloscope can calibrate itself by signal-path compensation. The self-calibration function is also used to calibrate DC offset of the A/D converters depending on the ambient-temperature change. This function is useful in multi-bit sampling.

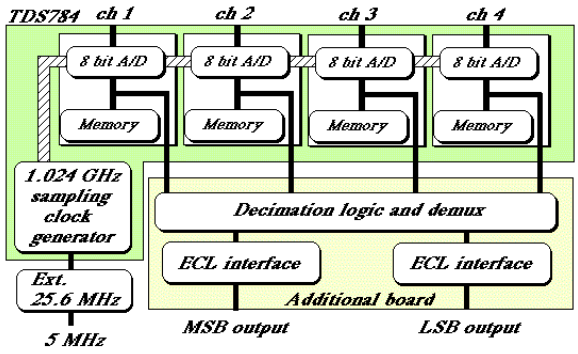

Figure 1. Block diagram of the data acquisition system.

2. ATM-interface unit

The ATM interface has a real-time clock phase-locked to the data clock of the giga-bit sampler. The data input from the giga-bit sampler are formatted and a time code is inserted. Channel selection (1/2/4 ch) and quantization-bit selection (1 or 2 bit) are performed in the formatting section. The rate of outputting data to the recorder or ATM line is selected from four rates ranging from among 256 to 2048 Mbps.

3. Parallel data processing

In VLBI observations, we can obtain the information about the station position and source's structure by cross-correlation using signals received at each station. In one-bit sampling, the sampled data are displayed as "1" or "0", which express a positive or a negative signal in analog. This simplified 1-bit signal also simplifies the correlation circuits, that is, the correlation is done by EXNOR (exclusive NOR) and counters.

In the current correlation processing algorithm, signal processing is bit-serial. The speed of correlation is limited by the speed of the device, and as a result, the device speed limits observing the (channel) bandwidth. This algorithm is not effective in astronomical applications. To overcome this problem, I developed a new correlation processing algorithm for parallel processing.

When designing a correlation processor, we must take into account delay tracking, fringe stopping, and 90-degree phase-jump. Parallel processing enables speeding up the current serial-processing algorithm. The circuit consistes of buffer memories, parallel shift registers and bit selectors. The buffer memories and shift registers works in toggle op-

Table 1. The results of self-calibration.

	ch1		ch2		ch3		ch4	
Range	linear.	offset	linear.	offset	linear.	offset	linear.	offset
mV/div		mV		mV		mV		mV
50	1.0040	0.033	1.0045	0.031	1.0019	1.323	1.0044	0.344
100	1.0041	0.241	1.0037	−0.455	1.0021	1.158	1.0056	−0.619
200	1.0055	−3.707	1.0061	−3.179	1.0035	−2.318	1.0045	−1.868

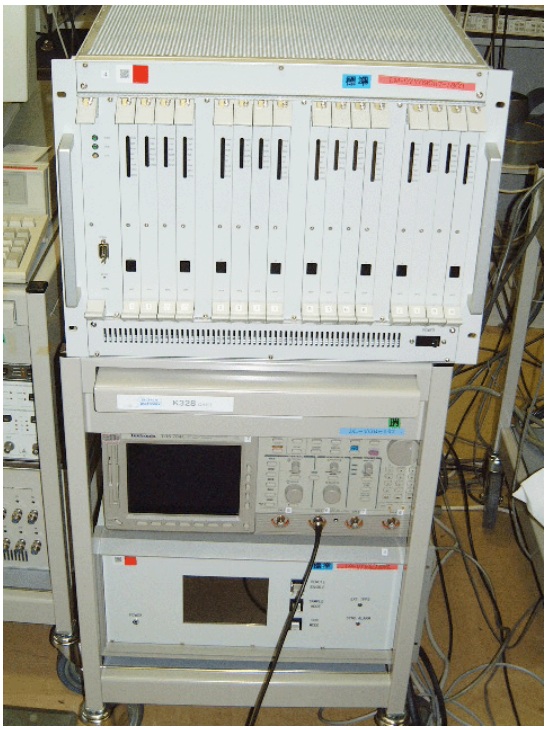

Figure 2. Picture of giga-bit system (Upper: giga-bit correlator, middle: sampler (TDS-784), lower: ATM interface).

eration. Bit selectors realize a one-bit step delay tracking.

3.1 Parallel integration

A simple real correlator/integrator consists of shift registers and an EXNOR (exclusive NOR). Correlated values are integrated by counters. Three-level approximation of the fringe signal is shown by using 2-bit signals. In these signals, one bit is a sign bit and the other is a blank-control bit. The sign bit is used for fringe stopping, and the blank-control bit is used for controlling integration. Integration of parallel data by using counters is inefficient. We introduced a matrix table in the ROM for the integration of parallel data. The parallel correlated data after fringe stopping and the blank-control bits are sent to a matrix calculator using the matrix table in the ROM. Integration circuit of each lag has a 31-bit-accumulator.

3.2 Data synchronization

In real-time correlation, the correlator is equipped with a function for automatic data synchronization with no external units. Time stamps composed of year, day, hour, minute, second, and a SYNC code used in time-code recognition are inserted into the data at regular intervals. To absorb the transmission-path delay, signals are stored in the buffer memory when a time stamp is received. This time stamp is generated by the ATM-interface unit. Readout starts immediately after the time stamps from all observation stations arrive, which enables the timing to be synchronized. Because the data are outputted to the correlation part after the timing is synchronized, the output data for each station are correct up to the time of the time stamp. The size of the buffer memory is 64 Mbits/ch.

4. System evaluation

To evaluate the giga-bit system we developed, a number of tests were conducted.

4.1 Results of signal-path compensation (self-calibration)

The measured results of DC-offset calibration and linearity are shown in Table 1. The frequency characteristics of the gain variation of the input amplifier are better than 1 dB ($<$ 500 MHz) and 2 dB (500 $<$ freq $<$ 1000 MHz). The sampling is usually done at the Nyquist rate, $1/(2 \times \mathrm{BW})$, where BW is the bandwidth of a channel. This is optimal for geodetic VLBI observations of wideband continuum radio sources. The sampling is done in one or two bits. It is inefficient to use quantization of more than two-bits in a signal-to-noise ratio per bits recorded. In a 1-bit/sample, for example, the sample value is chosen to be 0 if the voltage at the sampling instant is $<$ 0 V, and 1 if the voltage is $>$=0 V. For a 2-bit (4-level)/sample, the threshold voltage is chosen at 0.95 σ (σ= 0.224 V for a 0-dBm input signal), and each sample is assigned one of four possible values. The threshold voltage

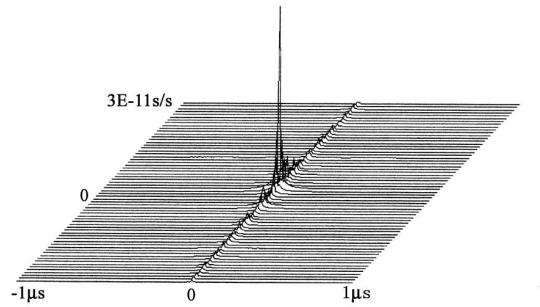

Figure 3. Simulated result by using a wavefront clock simulator.

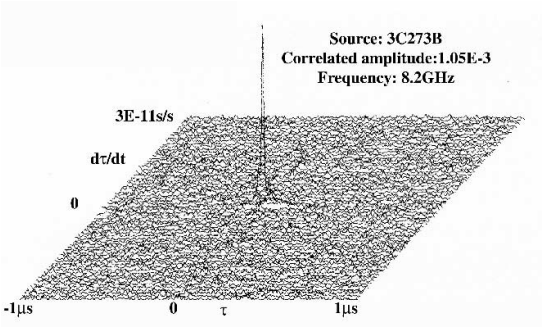

Figure 4. Result of Koganei-Kashima baseline real-time VLBI experiment.

is the same as that in the two-division range of an oscilloscope display. A 100-mV/div range is used for 0-dBm analog signals.

4.2 Correlator specifications

A photograph of the giga-bit system is shown in Fig. 2. The number of parallel data bits is 64. The maximum processing speed is 2048 bps/ch, and it is a four-channel correlator. Each channel has 1024 complex lags.

4.3 Correlation by using a wavefront clock fringe simulator

White noise from a noise diode is converted to a signal received from a star as if observed at the target station by using a wavefront clock system. If one of the divided RF noises is acquired by using a normal VLBI system and the other is acquired by a wavefront clock system, we can obtain VLBI data as if they were obtained at two different stations, that is a VLBI fringe data simulator. The simulator generated virtual VLBI station data that we used to check the work of the giga-bit correlator. One of the simulated results is shown in Fig. 3.

4.4 Real-time fringe detection using an ATM network

After a transmission test through the ATM line, a real-time experiment was carried out between Koganei and Kashima KSP stations. The IF signal was down-converted to a wide-bandwidth video signal by using a KSP local oscillator. The wide-bandwidth video signal was sampled by the giga-bit sampler, and then formatted by the ATM interface-unit. The formatted signal was transmitted from Kashima to Koganei via the ATM line. After that, correlation processing was performed. The experimental result is shown in Fig. 4. As a result, we could obtain fringes with high SNR.

Present status and future problems of the orbit determination for Nozomi spacecraft

Makoto Yoshikawa[1] (*makoto@pub.isas.ac.jp*), **Mamoru Sekido**[2], **Noriyuki Kawaguchi**[3], **Kenta Fujisawa**[3], **Hideo Hanada**[4], **Yusuke Kono**[4], **Hisashi Hirabayashi**[1], **Yasuhiro Murata**[1], **Satoko Sawada-Satoh**[1], **Kiyoaki Wajima**[1], **Yoshiharu Asaki**[1], **Jun'ichiro Kawaguchi**[1], **Hiroshi Yamakawa**[1], **Takaji Kato**[1], **Tsutomu Ichikawa**[1], **and Takafumi Ohnishi**[5]

[1] *Institute of Space and Astronautical Science (ISAS)*
3-1-1 Yoshinodai, Sagamihara, Kanagawa 229-8510, Japan
[2] *Kashima Space Research Center*
Communications Research Laboratory (CRL)
893-1 Hirai, Kashima, Ibaraki 314-0012, Japan
[3] *National Astronomical Observatory (NAO)*
2-21-1 Osawa, Mitaka, Tokyo 181-8588, Japan
[4] *Mizusawa Astrogeodynamics Observatory*
National Astronomical Observatory
2-12, Hoshigaoka, Mizusawa, Iwate 023-0861, Japan
[5] *Fujitsu Limited*
3-9-1 Nakase, Mihama-ku, Chiba-shi, Chiba 261-8588, Japan

Abstract: After the launch on July 3, 1998 from Kagoshima Space Center (KSC), Nozomi spacecraft is now on going to Mars in the interplanetary space. The orbital determination (OD) group of Institute of Space and Astronautical Science (ISAS) has been carrying out the works of orbital determination using the radiometric data taken mainly in Usuda Deep Space Center (UDSC). For the future orbit navigation of Nozomi, we may need new methods, such as the delta-VLBI (Very Long Baseline Interferometry) technique, because in some part of the orbital phase the range data cannot be taken. Therefore, the OD group of ISAS and some research groups of VLBI of ISAS and other institutes have started investigating the application of delta-VLBI method to the orbit determination of Nozomi. In this paper, we summarize the present status and future problems of the orbit determination for Nozomi spacecraft.

1. Introduction

Nozomi (Fig.1) is the first Japanese spacecraft that goes to the planet Mars. ISAS already launched several spacecraft that went into interplanetary space, such as "Sakigake" and "Suisei". From the point of orbital determination (OD), Nozomi is quite different from these previous ones because the requirement for the OD accuracy is much higher. The maximum distance between Nozomi and the earth is about 5×10^5 km in the near-earth phase and about 3×10^8 km in the interplanetary phase. This indicates that the accurate OD is much more difficult in the interplanetary phase than in the near-earth phase. The OD group in ISAS has been trying to obtain the much more accurate orbit for Nozomi. However, we find that there are several difficult problems in front of us. We will mention these problems briefly in the section 4.

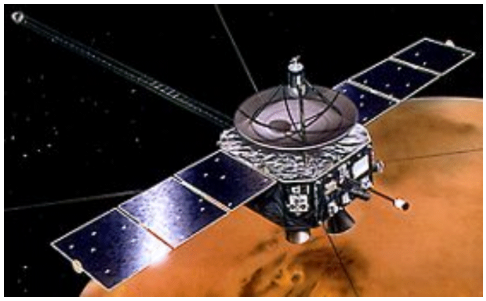

Figure 1. Nozomi spacecraft

Up to now (November 2001), there are several events that are very critical to the orbital determination of Nozomi. They are as follows:

03 July 1998	:	launch
24 Sept. 1998	:	1st lunar swingby
19 Dec. 1998	:	2nd lunar swingby
20 Dec. 1998	:	Earth swingby (Trans Mars Insertion)
until March 1999	:	There are many maneuvers (ΔVA1$\sim\Delta$V10)
02 May 1999	:	small gas leak
05 July 1999	:	S-band downlink stopped
22-23 June 2000	:	maneuver (ΔV11)

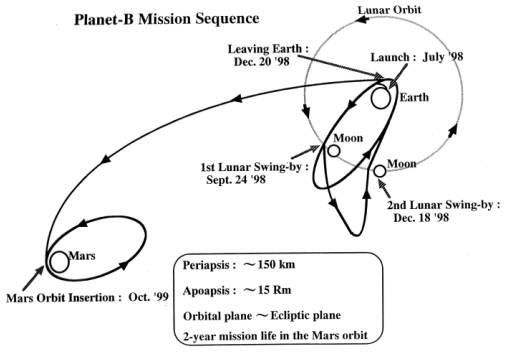

Figure 2. Original mission plan

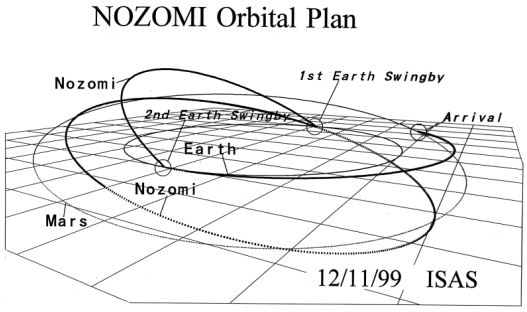

Figure 3. New orbital plan

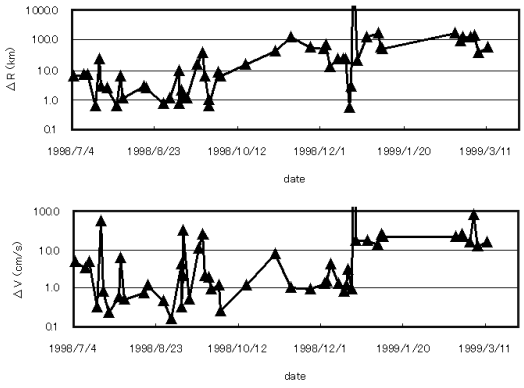

Figure 4. The difference of the orbit determination between ISAS and JPL. R is position and V is velocity.

At the time of Trans Mars Insertion on 20 Dec. 1998, there was a problem, so the original plan (Fig.2) could not be achieved. The new orbital plan was made (Fig.3). In this new plan, Nozomi will have two more swingbies by the earth (Dec. 2002 and June 2003), and will arrive at Mars at the beginning of 2004.

Here, we have another problem. We cannot receive range data during the two earth swingbies because now we cannot use S-band downlink. Therefore, we must consider the alternate method, and that is the delta-VLBI method, which is mentioned in the section 5.

2. Method of orbit determination

In ISAS we have been developing the orbital determination software called ISSOP (ISAS Orbit Determination Program) from more than 15 years ago. This software was first used for the mission of Sakigake and Suisei, which were launched in 1985 to the comet Halley. The next mission that ISSOP was used was Hiten, which was launched 1990. Since then, we have continued modifying ISSOP to carry out more accurate OD ([1],[2]).

ISSOP is the software for orbital determination using radiometric data (range and range-rate) and angle data. For the deep space mission, only the range and range-rate data are used. ISSOP takes into account the perturbations of the sun, moon, planets (from Mercury to Saturn), the nonspherical component of potential around planets, the solar radiation pressure, the drag force of atmosphere, and other small forces such as gas leak. ISSOP uses the least square method for orbital estimation.

As for Nozomi spacecraft, we tried to modify ISSOP in several point to get much accurate orbits of Nozomi. In the section 4, we show what we have done and are trying to do to carry out much accurate OD.

3. Accuracy of orbital determination

The most difficult point in the work of OD for spacecraft is that we can never know the true orbit of each spacecraft. Therefore in order to check accuracy of our OD, we carried out following checks:

(a) check O-C (O : observation, C : calculation)
(b) check the self consistency
(c) compare with other results obtained by using different software
(d) compare with other results obtained by other groups

As for (a), if the values of O-C are distributed randomly around zero, then we think our orbital determination is good and that only the noise component is shown in the distribution of O-C. As for (b), we did as follows. The orbital determination is carried out for certain period which is divided by some events such as shown in the section 1. Then we can compare the determined values of successive periods for the epoch just between these two periods. If the difference is small, then our analysis would be reliable. As for (c), we do not have another software which is comparable to ISSOP at present, so we cannot use this method fully. But we check the results obtained by ISSOP by other programs as far as we can. As for (d), we compare our results with those obtained by Jet Propulsion Laboratory (JPL), if possible.

The detailed analyses are omitted here and we show one of our results. Fig. 4 shows the results of comparison between the results of ISAS and JPL for the period of from the launch to March 1999. In this period, Nozomi spacecraft was not so far from the earth and the maximum distance is less than 2×10^7 km. Roughly speaking, this figure indicates that the accuracy (1-sigma) of position is from 1 km to 100 km, and that of velocity is 1cm/s

to 10cm/s. The accuracy varies depending on the phase of orbit.

As for the interplanetary phase, the accuracy is from hundreds km to thousands km in position, and up to 1m/s in velocity. In this case the accuracy also strongly depends on the phase of orbit.

4. Problems up to now

In the process of OD for Nozomi, there are four major difficulties that we encountered up to now. They are as follows:

(a) modulation by spin
(b) solar radiation pressure
(c) small force caused by re-orientation maneuvers
(d) solar conjunction

We just summarize here what we have done up to now for these problems.

Since Nozomi is rotating about 7 rpm, there are some spin effects in the observed data of range and range-rate. In order to carry out the accurate OD, we should remove the effects of spin. We obtained a function that simulates the effects of spin, and eliminated them. After the elimination of spin, the accuracy of OD became a little better.

As for the solar radiation pressure, we modified our previous model largely. Our previous model for the solar radiation pressure was a quite simple one, where we assume one plate instead of spacecraft itself and the direction of the radiation force is the same as that of the incoming radiation. In our new model, we assumed that the spacecraft consists by several panels, which are both perpendicular and parallel to the spin axis of the spacecraft. We consider the spin motion to estimate the radiation force and we also took into account not only the force along the direction of incoming beam but also the force perpendicular to the panels of spacecraft. By these modifications, the accuracy of our OD becomes rather better. However, we should still improve our model to obtain much better orbits.

Next, we mention about the small force caused by re-orientation maneuvers. In fact, such small force was not expected before the launch but we recognized that there are variations about 1 mm/s in the range-rate data when re-orientation maneuvers occurred (Fig.5). After the trouble of S-band downlink, the re-orientation maneuvers occurred much more frequently, because X-band, which has narrower beam size, was used for downlink. Therefore, this small force by re-orientation has a large effect to the OD of Nozomi. We have tried several methods to estimate this small force, but we have not reached satisfied results yet.

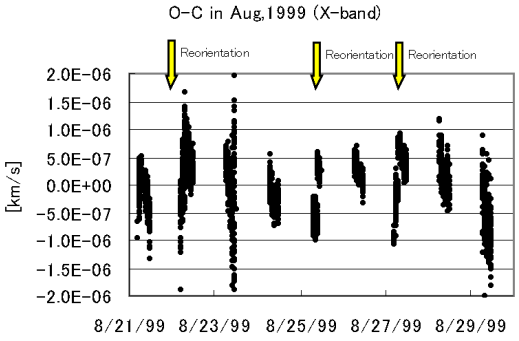

Figure 5. Small force caused by re-orientation

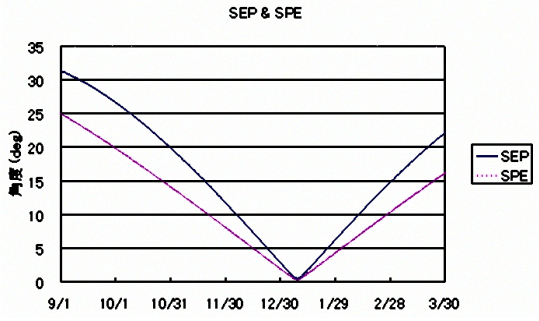

Figure 6. Variations of the angles from 2000 to 2001. (SEP: Sun-Earth-Nozomi, SPE: Sun-Nozomi-Earth)

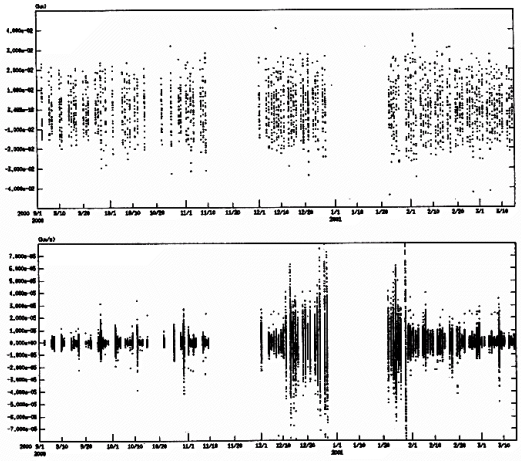

Figure 7. Noise level in range (upper) and range rate (lower) from September 2000 to March 2001.

Finally there is a problem caused by the conjunction. At the beginning of the year 2001, the angle Sun-Earth-Nozomi became very small (Fig.6). This means that Nozomi was observed very close to the sun. When the conjunction occurs, we cannot establish the link between Nozomi and the ground stations. In fact, the communication was stopped for about three weeks around the conjunction. In addition to this, the range and range rate data are

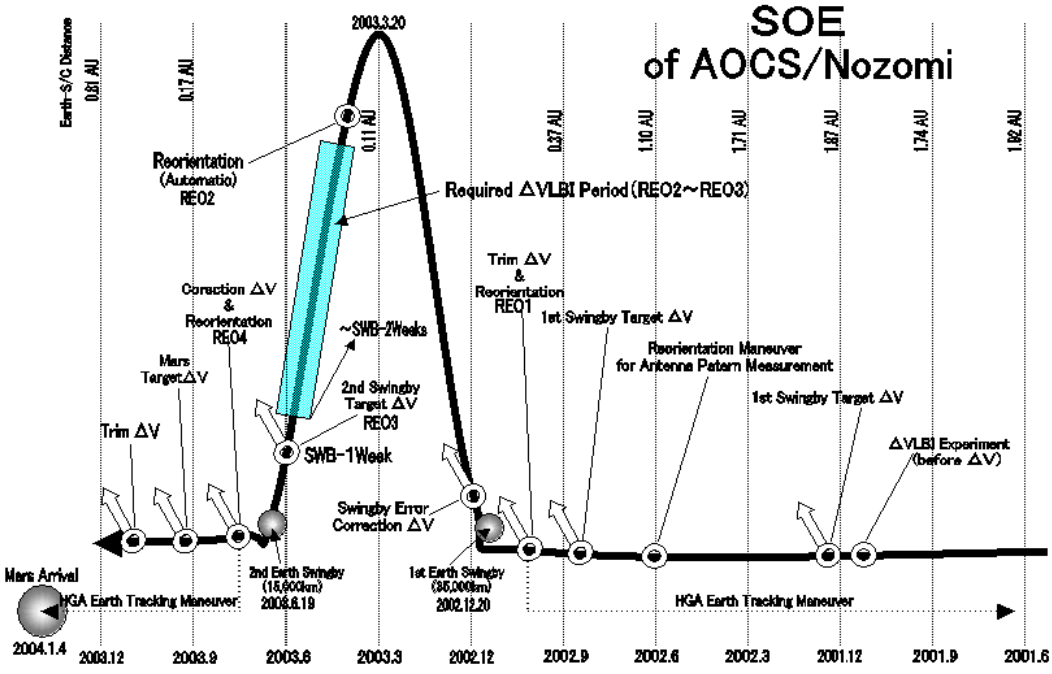

Figure 8. Nozomi navigation plan from 2001 to its arrival to Mars

affected by noise. In Fig.7, the noise level is shown for both the range and the range rate data. From this figure, the noise level of range rate becomes very large near the conjunction. As for the range, the effect of conjunction seems small. During the period of conjunction, the accuracy of orbit determination becomes worse. We are now trying to overcome this difficulty.

5. Problem in future

In this final section, we will discuss about one of the future problems related to the navigation of Nozomi. The principal issue for the navigation of Nozomi spacecraft near future is the two earth swingbies (Fig.8). As it is already mentioned, we cannot receive range data in almost all the period between these two swingbies, because we cannot use S-band downlink now. This means that we cannot use range data for about a half year. Although we can get the range rate data, this is a very serious problem for OD. The high accuracy of OD is required especially for the second earth swingby. Therefore, now we have started discussion about using delta-VLBI technique in OD of Nozomi. Fortunately there is VSOP (VLBI Space Observatory Program) group in ISAS and also there are research groups for VLBI in Communications Research Laboratory (CRL) and National Astronomical Observatory (NAO) in Japan. The researchers from these organizations have gathered in a working group and started discussing the possibility using delta-VLBI. The detailed discussions will be reported in the paper by Sekido et al in the future issue.

References

[1] T.Nishimura, T.Kato, and A.Ushikoshi : Tracking of Sakigake and Suisei and Development of Software package ISSOP for Orbit Determination. ISAS report NO.42, 1986.

[2] T.Nishimura, T.Ichikawa, A.Ushikoshi, H.Kosaka : Tracking of MUSES-A 'HITEN' and description of software package ISSOP for orbit determination. ISAS report NO.70, 1991.

Possibility of Phase-Referencing Observations in the Next Generation Space VLBI Mission

Hisashi Hirabayashi[1] (*hirax@vsop.isas.ac.jp*), **Yasuhiro Murata**[1], **Edward Fomalont**[2], **Robert Preston**[3], **David Murphy**[3], **Hideyuki Kobayashi**[4], **Philip G. Edwards**[1], **and Yoshiaki Asaki**[1]

[1] *The Institute of Space and Astronautical Science 3-1-1 Yoshinodai, Sagamihara, Kanagawa, 229-8510 Japan*
[2] *National Radio Astronomy Observatory Edgemont Road, Charlottesville, Virginia, USA*
[3] *Jet Propulsion Laboratory, NASA Oak Grove Drive, Pasadena, CA, USA*
[4] *National Astronomical Observatory 2-21-1 Osawa, Mitaka, Tokyo, 181-8588 Japan*

Abstract: Following the success of the VLBI Space Observatory Programme (VSOP), a next generation space VLBI mission is currently being planned. Higher observing frequencies, cooled receivers, increased bandwidths and larger telescope diameters will result in gains in resolution and sensitivity by factors of ∼10 over the VSOP mission. The use of "phase-referencing" by fast switching between a calibrator source and the target source is now under study. This technique would permit the imaging of sources more than a factor of 20 weaker.

1. Introduction to Next Generation Space-VLBI Mission VSOP-2

Space VLBI synthesizes a telescope larger than the Earth. ISAS's launch of the HALCA satellite in 1997, as part of the VLBI Space Observatory Programme (VSOP), has allowed sub-milli-arcsecond–scale imaging at 1.6 GHz and 5 GHz [*Hirabayashi et al.,* 1998, 2000a]. In addition, successful detection of space-ground fringes at 22 GHz confirmed that there will be no major problems extending space VLBI to shorter wavelengths in the future. Planning for a next generation space VLBI mission, currently designated as VSOP-2, is well underway [*Hirabayashi et al.,* 2000b]. The VSOP-2 spacecraft will have a 10m-class antenna with cryogenically cooled low-noise receivers and a downlink data rate of at least 1 Gbps, resulting in an improvement of an order of magnitude in interferometer sensitivity over the VSOP mission. Observing frequencies up to 43 GHz will allow high angular resolution observations of the optically thin emission in many AGN cores. An angular resolution of ∼25 micro-arcseconds at 43 GHz will be achievable, corresponding to ∼10 Schwarzschild radii at the distance of M87.

The VSOP-2 science goals include: Study of emission mechanisms in conjunction with the next generation of X-ray and gamma-ray satellites; full polarization studies of magnetic field orientation and evolution in jets, and measurements of Faraday rotation towards AGN cores; high linear resolution observations of nearby AGN to probe the formation and collimation of jets and the environment around supermassive black holes; and the highest resolution studies of spectral line masers and megamasers, and circum-nuclear disks.

Submission of the VSOP-2 proposal will take place within the next year. Launch on an ISAS M-V rocket could be as early as 2008.

2. Current design parameters of VSOP-2 Spacecraft and Ground support System

The VSOP-2 spacecraft will be three-axis stabilized, and will probably employ an off-axis paraboloid antenna with 10-12 m diameter. The observing frequency will be 5 or 8 (or, 5 to 8, if possible), 22, and 43 GHz, and the highest frequency places stringent requirements on the surface accuracy of the antenna with mesh surface (∼0.3 mm r.m.s.). The VSOP-2 satellite will be placed in an elliptical orbit with an apogee height of ∼30,000 km and a perigee height of ∼1,000 km, resulting in a period of ∼8 hours. The VSOP-2 satellite will detect LCP and RCP, and will use cryogenic coolers to reduce the system temperature by a factor of ∼3 compared to HALCA. Observing requires a two-way link between the satellite and a tracking, and the frequency bands assumed are 37–38 GHz band for wideband down link with 1 Gbps or more, and 40 GHz for uplink. The WG has researched and improved the following items.

3. Enhancing the mission with Phase-Referencing Capability

Sensitivity is limited by the short coherence time which is predominately caused by atmospheric fluctuations above the ground telescopes. "Phase-referencing" observations improve sensitivity by extending the coherent integration time, and can also provide capability for astrometric observations.

For the VSOP mission, phase referencing was not considered in the initial satellite designed, and a phase-referencing working group was formed in the VSOP mission with Dr. Richard Porcas (MPIfR, Germany) as the chairperson. Phase-referencing observations have successfully been carried out [*Porcas et al.,* 2000; *Guirado et al.,* 2001].

Guirado et al, for example, made a successful phase referencing observation of the quasar pair 1342+662/1342+663 with 4.8 minute of arc separation with common beam observation at 5 GHz.

The possibility of enhancing the mission with phase-referencing capability is now being extensively studied. The VERA array of the National Astronomical Observatory of Japan, which consists of four 20 m antennas with dual beam systems for phase-referencing observations, will provide variable experience in developing phase referencing techniques for VSOP-2, and could be one of a good collaborating telescope arrays.

4. Estimates of Phase-Referencing Performance

A rough estimate of the coherence times and the detection thresholds are;

10 min	and	4.9 mJy	(at 5 GHz),
6 min	and	9.4 mJy	(8 GHz),
2 min	and	38 mJy	(22 GHz) and
1 min	and	94 mJy	(43 GHz),

using the nominal sensitivity parameters of the design of VSOP-2. Without phase referencing these are the minimum flux densities of sources that can be imaged with VSOP-2. The use of water vapor radiometers to measure directly the short term changes in the tropospheric path length may help extend the coherence time considerably and lower the detection thresholds. If the switching time between observations of the target source and nearby calibrator source is be less than the above times, then phase referencing techniques can be used.

Initial estimates of the gain achieved by adding a phase-referencing capability to the VSOP-2 satellite have been made. The density of radio sources in the sky is well-known from ground radio surveys. From the VSOP 5 GHz survey, we find that about 10% to 20% of the sources have significant correlated flux density at 30,000 km baselines. With the nominal mission parameters affecting VSOP-2 sensitivity, we find that the average separation between target and calibrator sources, and the primary beam size become:

1.3 degrees	(at 5 GHz, 0.31 degree FWHP),
2.2 degrees	(8 GHz, 0.18 degree FWHP),
8.3 degrees	(22 GHz, 0.07 degree FWHP) and
14.9 degrees	(43 GHz, 0.04 degree FWHP).

With successful phase referencing, the estimate of 3 times rms image detection sensitivity in an 12-hour phase-referencing observation with VLBA is: 0.15 mJy (at 5 GHz), 0.23 mJy (8 GHz), 0.54 mJy (22 GHz) and 0.94 mJy (43 GHz). Thus, sources which are more than a factor of 20 under the detection thresholds can be imaged with VSOP-2.

Phase referencing is easier at lower frequencies because the separation between target and calibrator sources is only a few primary beam widths or a few degrees. With the nominal VSOP-2 parameters, phase-referencing below 8 GHz looks possible but become difficult at 22 and 43 GHz.

With realistic extrapolations to present day receiving technology, we may be able to design a mission which is up to 30 times more sensitive than the nominal design by assuming larger launcher. Such an increase in sensitivity would decrease the target-source separation considerable, making and phase-referencing at 22 and 43 GHz possible.

5. Orbit Accuracy for Phase-Referencing Observations

For phase referencing observations ∼120 cm (5 GHz), 50cm (8 GHz), 6.5cm (22 GHz) and 1.8cm (43 GHz) accuracies are needed for our space-ground baseline. To detect H2O maser proper motion in Active Galactic Nuclei sources, a 2 cm orbit accuracy is needed. HALCA has been able to achieve 3-10 m orbit accuracy, and this may be the limit of 2-way Doppler tracking.

Better orbit determination accuracy can be achieved by adding GPS receivers and a high precision accelerometer, even though the GPS illumination coverage is limited in our space-VLBI orbit. Simulations performed at JPL for our orbit gives ∼2cm accuracy by installing a JPL-developed GPS receiver package (2.5 kg, 20 W) including a 3-dimensional accelerometer (20 kg, 8 W) with 0.1 mm/s/s accuracy.

6. Possible Spacecraft Design for Phase-Referencing Observations

One method of phase-referencing is the nodding of the whole spacecraft quickly between the calibrator and target sources. Such fast slewing of the spacecraft may be possible with the use of large momentum reaction wheels (RWs), and the addition of Control Moment Gyroscopes (CMGs). The configuration with 2 CMGs and 4 RWs seems to be possible without too much mass and power budget consumption, even though the control logic becomes considerably complicated.

Not only the maneuvering time but also spacecraft settling time must be considered in connection with the antenna-spacecraft structure and attitude control logic. Two minutes settling time is observed in the case of HALCA is too long. VSOP-2 will have off-set antenna, and the larger antenna has strong impact on system design.

The nutating of sub-reflector, with little or no change in the orientation of the whole spacecraft, is another option to switch observations between calibrator and source. But, nodding is limited to separation angles to less than about 30 primary beamwidths in order to minimize the gain loss of the off-set beam. However, the switching is extremely fast with little settling time necessary.

A two-beam system, as employed for VERA, has severe impacts on the spacecraft design and is likely to be too difficult to merit serious consideration.

Generally speaking, as the current VSOP-2 assumes an M-V launcher, the payload budget places a strong limitation on the design, however, studies are still in progress for including a phase-referencing capability.

There is another area for greatly increasing the mission capability. Two spacecraft mission will have better (u,v) coverage in terms of direction and observing epoch and more baseline length. This might come after VSOP-2 or in conjunction with a VSOP-2 type mission with larger international participation.

References

Guirado, J.C., Ros, E., Jones, D.L., Lestrade, J.F., Marcaide, J.M., Perez-Torres, M.A., and Preston, R.A., 2001, Astronomy and Astrophysics, 371, 766-770

Hirabayashi, H. et al. 1998, Science, 281, 1825 and erratum 282, 1995

Hirabayashi, H. et al. 2000a, PASJ, 52, 955

Hirabayashi, H. et al. 2000b, in Astrophysical Phenomena Revealed by Space VLBI, ed. H. Hirabayashi, P.G. Edwards, and D.W. Murphy (ISAS), 277

Porcas, R.W., Rioja, M.J., Machalski J., and Hirabayashi, H. 2000, in Astrophysical Phenomena Revealed by Space VLBI, ed. H. Hirabayashi, P.G. Edwards, and D.W. Murphy (ISAS), 245

VERA description paper

"IVS CRL Technology Development Center News" (IVS CRL-TDC News) published by the Communications Research Laboratory (CRL) is the continuation of "International Earth Rotation Service - VLBI Technical Development Center News" (IERS TDC News) published by CRL. In accordance with the establishment of the International VLBI Service (IVS) for Geodesy and Astrometry on March 1, 1999, the function of the IERS VLBI technical development center was taken over by that of the IVS technology development center, and the name of center was changed from "Technical Development Center" to "Technology Development Center".

VLBI Technology Development Center (TDC) at CRL is supposed

1) to develop new observation techniques and new systems for advanced Earth's rotation observations by VLBI and other space techniques,
2) to promote research in Earth rotation using VLBI,
3) to distribute new VLBI technology,
4) to contribute the standardization of VLBI interface, and
5) to deploy the real-time VLBI technique.

The CRL TDC newsletter (IVS CRL-TDC News) is published biannually by CRL.

This news was edited by Tetsuro Kondo and Yasuhiro Koyama, Kashima Space Research Center, who are editorial staff members of TDC at the Communications Research Laboratory, Japan. Inquires on this issue should be addressed to T. Kondo, Kashima Space Research Center, Communications Research Laboratory, 893-1 Hirai, Kashima, Ibaraki 314-0012, Japan, TEL : +81-299-84-7137, FAX : +81-299-84-7159, e-mail : kondo@crl.go.jp.

Summaries of VLBI and related activities at the Communications Research Laboratory are on the World Wide Web (WWW). The URL to view the home page of the Radio Astronomy Applications Section of the Kashima Space Research Center is : **"http://www.crl.go.jp/ka/radioastro/"**. The URL to view the Keystone project's activity is **"http://ksp.crl.go.jp/"**.

IVS CRL TECHNOLOGY DEVELOPMENT CENTER NEWS No.19, November 2001

International VLBI Service for Geodesy and Astrometry
CRL Technology Development Center News
published by
Communications Research Laboratory, 4-2-1 Nukui-kita, Koganei, Tokyo 184-8795, Japan